Minimally invasive myocardial infarction model recapitulates patient immune responses and reveals a pathogenic role for immature neutrophils

Zoe Möller-Ramon[1,*], Anna Kaltenbach[1,*], Sarah-Lena Puhl[1,2], Immanuel Kwok[3], Florian Sicklinger[4,5], Yvonne Jansen[1], Annick Ernst[1], Katrin Nitz[1,6], Maximilian J. Schloss[1,7,8], Florian Leuschner[4,5], Mark Yan Yee Chan[9,10], Christian Weber[1,11,12], Sabine Steffens[1,11,13,#] and Johan Duchêne[1,11,#].

[1]Institute for Cardiovascular Prevention (IPEK), Ludwig-Maximilians University Munich (LMU), Pettenkoferstraße 9, 80336 Munich, Germany.
[2]Comprehensive Heart Failure Center, University Clinic Würzburg, Würzburg, Germany.
[3]Singapore Immunology Network (SIgN), Agency for Science, Technology and Research (A*STAR), 8A Biomedical Grove, Immunos, Singapore 138648, Republic of Singapore.
[4]Department of Internal Medicine III, University Hospital Heidelberg, Germany.
[5]German Centre for Cardiovascular Research (DZHK), Heidelberg, Germany.
[6]Department of Cardiovascular Medicine and Immunology, Mayo Clinic, Rochester, MN, US
[7]Center for Systems Biology, Massachusetts General Hospital and Harvard Medical School, Boston, MA, USA.
[8]Department of Radiology, Massachusetts General Hospital and Harvard Medical School, Boston, MA, USA.
[9]Department of Cardiology, National University Heart Centre, Singapore.
[10]Department of Medicine, Yong Loo-Lin School of Medicine, Singapore.
[11]German Center for Cardiovascular Research (DZHK), Partner Site Munich Heart Alliance, Pettenkoferstraße 8a, 80336 Munich, Germany.
[12]Cardiovascular Research Institute Maastricht, University of Maastricht, Universiteitssingel 50, 6229 ER, Maastricht, The Netherlands.
[13]Institute for Diabetes and Cancer, Helmholtz Zentrum Munich, Neuherberg, Germany.

[*]: contributed equally as first authors
[#]: contributed equally as senior authors
corresponding author: johan.duchene@med.lmu.de

Abstract

Myocardial infarction (MI) triggers a systemic neutrophil response, yet the roles of distinct neutrophil subsets in cardiac remodeling remain unclear. Studying this requires murine models that accurately mirror human neutrophil dynamics. Here, we show that a minimally invasive intact-chest MI model is more pathophysiologically relevant than the standard open-chest approach for investigating post-MI immune responses. In the open-chest model, surgical trauma disrupts bone marrow homeostasis, releases large numbers of immature neutrophils, and masks MI-specific immune mechanisms. In contrast, the intact-chest model preserves bone marrow integrity and induces only a modest rise in circulating immature neutrophils, closely reflecting MI patient profiles. We further demonstrate that accumulation of immature neutrophils in the infarcted heart exacerbates cardiac dysfunction. Beyond neutrophils, the overall cardiac immune landscape differs markedly between both models. Collectively, our findings establish the intact-chest model as superior for studying post-MI inflammation and reveal immature neutrophils as mediators of adverse cardiac remodeling.

Introduction

Myocardial infarction (MI), a leading cause of death and disability worldwide[1], triggers a complex inflammatory cascade that profoundly influences cardiac repair and patient outcomes[2-6]. Neutrophils represent the predominant early-responding leukocyte population recruited to the infarcted myocardium[2-12].

Neutrophils are produced in the bone marrow (BM) through granulopoiesis, a tightly regulated process in which myeloid precursors develop first into immature and then mature neutrophils[13-15]. Under homeostatic conditions, only fully mature neutrophils are released into circulation, while immature cells are retained in the BM. Following tissue injury, mature neutrophils are rapidly recruited and consumed at sites of inflammation[16]. To meet increased demand, the BM responds by releasing larger numbers of neutrophils, including immature cells. The presence of immature neutrophils in peripheral blood is known as "left shift" and can arise through different mechanisms, depending on the severity of the inflammatory stimulus. In moderate inflammation, stored mature neutrophils and a limited proportion of immature neutrophils are mobilized, mainly under the influence of granulocyte colony-stimulating factor (G-CSF), a well-established regulator of neutrophil release[17]. In severe inflammation, sustained cytokine signaling triggers "emergency granulopoiesis"[18-20], a rapid and amplified neutrophil production process in which cells are generated faster than adequate maturation allows[20-22]. Consequently, immature neutrophils are prematurely released and, in the most severe cases, may even outnumber mature neutrophils in the circulation.

Despite their clinical relevance, most studies on MI have examined neutrophils as a homogeneous population without distinguishing mature and immature subsets. Recent clinical studies have reported elevated circulating immature neutrophils in MI patients[23,24]. However, it remains unknown whether MI triggers emergency granulopoiesis, whether these immature cells infiltrate the infarcted heart, and whether they represent passive bystanders or actively influence post-infarction outcomes.

To address these questions, mouse MI models that closely mirror human immune responses, particularly those involving neutrophils, are needed. The widely used open-chest MI (oc-MI)

100 model involves surgical intervention[25-27] that induces systemic inflammation and may disrupt
101 BM homeostasis, potentially confounding studies of neutrophil response. Here, we compared
102 the ischemia-driven neutrophil response in the conventional open-chest approach with a
103 newly developed intact-chest MI (ic-MI) model[28], benchmarking both against human MI
104 immune responses. Our goal was to identify the model that most accurately reflects human
105 pathology, thereby enabling rigorous investigation of immature neutrophils in post-infarction
106 setting. Defining these mechanisms may reveal novel translational targets to improve post-
107 MI outcomes.

108 **Results**

109 **Presence of circulating immature neutrophils in AMI patients**

110 To validate recent reports of circulating immature neutrophil subsets in the context of acute
111 MI (AMI) in participants, we assessed neutrophil maturation status in peripheral blood
112 samples from an independent cohort of patients hospitalized for AMI (Fig. 1A-B and Extended
113 Data Fig. 1). Flow cytometric analysis performed on peripheral venous blood obtained 24-48h
114 from the time of symptom onset revealed a marked increase in circulating immature $CD10^{-}$
115 neutrophils (iNeu), comprising approximately 10% of the total neutrophil pool compared to
116 roughly 1% in healthy donors (Fig. 1C-D). This expansion was further evidenced by the
117 increased proportion of $CD10^{-}$ immature neutrophils among total $CD45^{+}$ leukocytes (Fig. 1E)
118 and elevated absolute counts of $CD10^{-}$ immature neutrophils in blood of AMI patients (Fig.
119 1F). In contrast, the fraction of $CD10^{+}$ mature neutrophils (mNeu) among $CD45^{+}$ leukocytes
120 remained unchanged (Fig. 1E), and their absolute counts were modestly elevated in these
121 AMI patients (Fig. 1F). These findings confirm the presence of circulating immature
122 neutrophils in AMI patients and suggest their release to be triggered by the infarction event.
123

124 **Open-chest surgery alters bone marrow homeostasis**

125 To test whether MI truly induces left shift and to explore the underlying mechanisms, we next
126 employed mouse models. First, we used the widely established oc-MI model (Fig. 2A) and
127 examined whether it recapitulates human pathology by assessing the presence of circulating
128 immature neutrophils following left anterior descending (LAD) artery ligation (Extended Data
129 Fig. 2A). We observed a profound increase in circulating $CD101^{-}$ immature neutrophils, which
130 constituted up to 80% of total neutrophils 24h post-MI, compared to 5% in steady state (Fig.
131 2B-C). This was associated with an elevation in $CD101^{-}$ immature and a corresponding
132 reduction in $CD101^{+}$ mature neutrophil numbers (Fig. 2D). Strikingly, sham-operated mice (oc-
133 SO) exhibited a comparable response to oc-infarcted mice, with a marked rise in $CD101^{-}$
134 immature neutrophils and a near-complete loss of $CD101^{+}$ mature neutrophils in circulation
135 (Fig. 2B–D).

136 To investigate the origin of this neutrophil shift, we next examined the BM compartment (Fig.
137 2E, Extended Data Fig. 2B). In both oc-MI and oc-SO groups, $CD101^{+}$ mature neutrophils were

138 virtually depleted at 24h post-intervention and replaced by CD101⁻ immature neutrophils
139 (Fig. 2F-G). Kinetic analysis revealed that all mature CD101⁺ neutrophils were rapidly
140 mobilized into circulation as early as 4h post-intervention, leaving immature neutrophils as
141 the predominant population in the BM (Extended Data Fig. 3A-B). This abrupt change explains
142 the overwhelming presence of immature neutrophils in both BM and peripheral blood at 24h.
143 BM composition and blood neutrophil distribution gradually returned to baseline within
144 seven days (Extended Data Fig. 3A-D). Additionally, CXCR2 expression, normally restricted to
145 mature neutrophils in steady state, was significantly upregulated on CD101⁻ immature
146 neutrophils in the BM of both oc-MI and oc-SO mice (Fig. 2H), indicating that surgical
147 intervention alters the phenotype of immature neutrophils.

148 Together, these findings demonstrate that open-chest surgery alone (i.e., thoracotomy)
149 triggers a severe immune response, disrupting granulopoiesis and causing a systemic shift in
150 neutrophil populations. This dramatic alteration of BM homeostasis, affecting both
151 composition and phenotype, significantly confounds the interpretation of immune responses
152 in the oc-MI model, thereby limiting its utility for studying MI-specific immune mechanisms.

153 **Intact-chest MI model recapitulates human-like neutrophil profile**

154 To minimize confounding factors introduced by the surgical procedure, we next employed the
155 recently developed intact-chest MI (ic-MI) model[28], which induces LAD artery occlusion
156 through minimally invasive coagulation (Fig. 3A). While mature neutrophil counts remained
157 unchanged, we found a modest but consistent increase in the percentage and number of
158 immature neutrophils in the circulation 24h post-MI (Fig. 3B-D), closely mirroring the
159 response observed in human patients (Fig. 1). Importantly, this increase was absent in the
160 respective sham-operated mice (ic-SO), allowing for a clearer distinction between MI-specific
161 and procedure-induced effects.

162 In the BM, the percentage and absolute numbers of mature and immature neutrophils were
163 comparable between ic-MI and ic-SO 24h post-intervention and baseline (BL) mice (Fig. 3E-
164 G). Additionally, CXCR2 expression on immature neutrophils remained unchanged after sham
165 (ic-SO) and MI (ic-MI) procedures (Fig. 3H). Thus, by avoiding surgical confounding effects, the
166 intact-chest model reveals that MI does not substantially alter BM neutrophil homeostasis.

167 To further dissect the divergent responses between the open-chest and intact-chest models,
168 we quantified circulating cytokines and chemokines 24h post-intervention using a multiplex
169 immunoassay (Fig. 3I). Sham surgery alone in the oc-model (oc-SO) was sufficient to induce a
170 robust upregulation of G-CSF, the key cytokine regulating neutrophil mobilization and
171 production, and CXCL1, a chemokine involved in neutrophil trafficking, in comparison to BL
172 controls. Similar levels of both mediators were detected in oc-infarcted (oc-MI) mice. In
173 contrast, these mediators remained unchanged in both ic-SO and ic-MI mice, relative to BL.
174 In addition, the chemokine CCL2 was also elevated in open-chest groups (oc-SO and oc-MI)
175 but remained at baseline levels in the intact-chest model (ic-SO and ic-MI). Furthermore,
176 inflammatory cytokines IL-6 and TNFα were increased in all groups except in ic-SO mice,
177 further underscoring the dominant contribution of the surgical trauma to the systemic
178 inflammatory response observed in the open-chest model.
179
180 Collectively, these results show that the intact-chest MI model does not provoke systemic
181 inflammation, preserves BM integrity, and more accurately mirrors the moderate increase of
182 circulating immature neutrophils observed in MI patients. By avoiding surgical confounding
183 effects, the ic-MI model thus provides a powerful tool for investigating MI-specific immune
184 responses, particularly those involving neutrophil subsets.
185
186 **MI triggers acute and rapid mobilization of immature neutrophils**
187 Next, we investigated the origin of immature neutrophils following MI in the intact-chest
188 model. Although we detected the presence of immature neutrophils in circulation 24h post-
189 MI (Fig. 3B-D), neither their egress from the BM (Fig. 3E-G) nor upregulation of neutrophil-
190 attracting molecules was observed at this time point (Fig. 3I). We therefore hypothesized that
191 MI may induce the mobilization of immature neutrophils at earlier stages.
192
193 Time-course analysis confirmed this hypothesis as plasma levels of G-CSF, CXCL1 and IL-6
194 measured by ELISA peaked at 4h after ic-MI compared to ic-SO controls and returned to
195 baseline levels within 24 hours (Fig. 4A-C). This early elevation of neutrophil chemoattractant
196 and mobilizer molecules was followed by a significant reduction of mature and immature
197 neutrophils in the BM at 12h post-MI (Fig. 4D–F and Extended Data Fig. 4A). Concurrently,
198 numbers of circulating neutrophils were higher in the ic-MI group than in ic-SO controls at

199 12h post-MI (Fig. 4G), with an increased proportion and absolute number of immature
200 neutrophils in circulation (Fig. 4H and I and Extended Data Fig. 4B and C).

201 In conclusion, these findings indicate that MI triggers a rapid, acute, and modest mobilization
202 of immature neutrophils from the BM. The intact-chest model thus enables temporal
203 resolution of neutrophil dynamics following MI and demonstrates that MI induces a left shift
204 through mobilization rather than increased granulopoiesis.

205 **Infiltration of immature neutrophils into the infarcted heart in ic-MI model**

206 Next, we aimed to characterize spatial neutrophil dynamics following MI. To this end, we
207 assessed neutrophil distribution across different organs 24h post-MI in the intact-chest model
208 using flow cytometry. As expected, we found that MI induced neutrophil accumulation
209 exclusively in thoracic organs, with the heart representing the primary site, followed by
210 mediastinal lymph nodes and the lung (Fig. 5A).
211
212 We then asked whether immature neutrophils infiltrate the infarcted myocardium. We
213 analyzed neutrophil subsets and found that both mature and immature neutrophils infiltrated
214 the infarcted heart (Fig. 5B and Extended Data Fig. 5). Infiltration of both populations peaked
215 between 12h and 24h post-MI and returned to baseline levels by day 5 (Fig. 5C). Consistent
216 with systemic observations, the ratio of immature to mature neutrophils in the heart mirrored
217 blood dynamics, with mature neutrophils approximately three-fold more abundant than
218 immature neutrophils in the infarcted myocardium (Fig. 4G–I and Fig. 5C).
219
220 We next investigated the spatial distribution of neutrophils in the infarcted heart using the
221 spatiotemporal MI map generated by antibody-based Sequential Immunofluorescence
222 (SeqIF; Lunaphore COMET)[29]. We found that 24h post-MI, MPO^+ neutrophils were absent
223 from remote areas (Fig. 5D inset i), sparse in border zones (Fig. 5D inset ii) and enriched in the
224 infarct core (Fig. 5D inset iii). Interestingly, within the infarcted region, neutrophils were
225 mainly localized beneath the endocardium and adjacent to the epicardium, suggesting their
226 infiltration through two distinct entry routes (Fig. 5D inset iii).
227 Together, flow cytometric and immunofluorescence analyses confirm that mature but also
228 immature neutrophils infiltrate the infarcted myocardium and reach the infarct area.

229 **A model to increase immature neutrophils recruitment to the infarcted heart**

230 We next aimed to investigate the contribution of immature neutrophils to cardiac
231 remodeling. However, this remains challenging as no specific tool currently exists to
232 selectively inhibit their mobilization or recruitment. To address this limitation, we sought
233 instead to enhance their recruitment to the heart. Given that G-CSF promotes BM egress of
234 immature neutrophils[15,17], we hypothesized that G-CSF treatment immediately after MI onset
235 would further increase their numbers in the circulation and subsequently in the infarcted
236 myocardium (Fig. 6A). Indeed, G-CSF-treated mice showed a marked increase in circulating
237 $CD101^{-}$ immature neutrophils 24h after MI, while mature neutrophil levels remained
238 unchanged (Fig. 6B–C). This was accompanied by greater accumulation of $CD101^{-}$ immature
239 neutrophils in the infarcted heart compared with PBS-treated controls (Fig. 6D–E). Analysis of
240 additional maturation markers confirmed the immature phenotype of these infiltrated
241 $CD101^{-}$ neutrophils, as they expressed lower levels of CD11b, CD62L and SiglecF than $CD101^{+}$
242 mature cells (Fig. 6F).

243 To assess the functional competence of $CD101^{-}$ immature neutrophils after cardiac
244 infiltration, we compared their effector functions to those of $CD101^{+}$ mature neutrophils. We
245 first measured their ability to generate reactive oxygen species (ROS) using the cell-
246 permeable probe dihydrorhodamine 123 (DHR123). Both mature and immature subsets
247 isolated from the infarcted heart displayed a comparable oxidative burst that largely
248 exceeded that of circulating mature neutrophils (Fig. 6G). Next, phagocytic capacity was
249 evaluated using pHrodo BioParticles, which fluoresce upon internalization and phagosomal
250 acidification. Immature neutrophils were able to internalize targets efficiently, although their
251 phagocytic activity was modestly lower compared to mature neutrophils (Fig. 6H). Altogether,
252 these results indicate that infiltrated immature neutrophils, despite being less differentiated,
253 possess functional myeloid effector activities (Fig. 6G-H).

254 In summary, G-CSF treatment in the ic-MI model selectively enhanced the recruitment of
255 functionally competent immature neutrophils into the infarcted heart, providing a valuable
256 approach to investigate their role in post-infarct cardiac repair.

257

258 **High immature neutrophil counts correlate with worsened cardiac performance and**
259 **adverse myocardial remodeling.**
260 To further clarify the impact of immature neutrophils on post-MI remodeling, we assessed
261 cardiac outcomes 28 days after ic-MI in G-CSF-treated mice (Fig. 7A). Echocardiographic
262 analysis revealed a more pronounced reduction in left ventricular ejection fraction (LVEF) and
263 a less negative global longitudinal strain (GLS) compared to PBS-treated controls (Fig. 7B-D),
264 indicating aggravated systolic dysfunction. Both left ventricular end-diastolic volume (LVEDV)
265 and left ventricular end-systolic volume (LVESV) were increased in the G-CSF–treated group
266 compared with the PBS-treated group (LVEDV: +29.7 µL, Hedges' g = 1.18, p = 0.14; LVESV:
267 +27.8 µL, Hedges' g = 1.35, p = 0.10) (Fig. 7E). Although these differences did not reach
268 conventional statistical significance ($p > 0.05$), the large observed effect sizes (Hedges' g > 1)
269 suggest a biologically substantial LV dilatation. Additionally, G-CSF-treated animals displayed
270 an elevated heart weight to tibia length (HW/TL) ratio (Fig. 7F) supporting persistent
271 inflammatory signaling and ongoing remodeling.

272 In line with these functional alterations, gene expression analysis in the infarcted hearts from
273 G-CSF-treated mice revealed changes of cardiac stress markers. This was characterized by
274 upregulation of *Nppa* (atrial natriuretic peptide, ANP), and a shift in myosin heavy chain
275 isoform expression, with decreased *Myh6* and increased *Myh7* levels (Fig. 7G). Moreover,
276 inflammation was sustained, as evidenced by higher *Il6* expression in hearts of G-CSF-treated
277 animals (Fig. 7G). Histological analysis further demonstrated adverse structural remodeling,
278 with a greater extent of fibrosis and larger scar size in hearts from G-CSF-treated mice
279 compared with vehicle controls (Fig. 7H–J).

280 Overall, these findings suggest that elevating immature neutrophil numbers during the early
281 post-MI phase leads to maladaptive remodeling with worsened cardiac performance at later
282 stages.

283 **Immune landscape of the infarcted heart**
284 Having characterized neutrophil dynamics following MI, we next investigated the responses
285 of other leukocyte populations. Previous studies using the open-chest model have reported
286 the presence and pathological roles of various immune cells in the infarcted heart[2-4].
287 However, the substantial systemic inflammation induced by the surgical procedure may

288 profoundly influence leukocyte recruitment and activation. The intact-chest model offers the
289 opportunity to more accurately define the immune landscape of the infarcted myocardium
290 under conditions that minimize surgical inflammation.

291 Using multiparametric flow cytometry, we quantified major immune cell populations in the
292 heart (Fig. 8A) and compared the kinetics of leukocyte infiltration between ic-MI and oc-MI
293 models (Fig. 8B-G). We found that neutrophil infiltration peaked at levels more than three-
294 fold higher in the oc-MI model compared to minimal-invasive ic-MI and remained elevated at
295 day 3 post-MI (Fig. 8B). Surprisingly, classical monocytes at day 1 post-MI were more
296 abundant in ic-MI hearts (Fig. 8C). In the later phase, macrophages increased dramatically in
297 oc-MI hearts at days 5 and 7, whereas their numbers remained largely unchanged in ic-MI
298 (Fig. 8D). In contrast, $CD11c^{+}$ cells were more prominent in ic-MI hearts peaking at days 3 and
299 5 before declining (Fig. 8E).

300 Lymphocyte dynamics also differed between models. In minimal-invasive ic-MI hearts, B cells
301 peaked at day 1 and returned to baseline by day 7; whereas in oc-MI hearts, B cell infiltration
302 began at day 3, progressively increased, and reached maximal accumulation at day 5,
303 plateauing through day 7 (Fig. 8F). We found that T cell recruitment was minimal in ic-MI
304 hearts during the first week post-MI, while in oc-MI hearts, T cell numbers peaked at day 3
305 and gradually declined thereafter (Fig.8G).

306 Overall, these data indicate that the immune landscape differs between the intact-chest and
307 open-chest MI models in magnitude, timing, and composition. These findings highlight the
308 value of adopting the minimal-invasive ic-MI model for future studies of post-MI immunity.

309 **Discussion**

310 Here, we provide the first comprehensive immunological validation of the minimally invasive
311 intact-chest MI model developed by Sicklinger and colleagues[28], and demonstrate that it
312 faithfully recapitulates the neutrophil response observed in MI patients. We further identify
313 immature neutrophils as contributors to post-MI outcomes. In addition, our findings highlight
314 significant limitations of the widely used open-chest MI model for studying immune
315 responses following MI.

316 The intact-chest MI model was originally developed to provide technical advantages and
317 improve animal welfare[28]. While its superiority in terms of speed and accuracy has been well
318 demonstrated, its impact on immune responses compared with the open-chest approach had
319 not yet been evaluated. By directly comparing the dynamics of the neutrophil response
320 between these two models, we found that surgical trauma profoundly reshaped neutrophil
321 maturation in the open-chest setting. Specifically, after an initial release of nearly all mature
322 neutrophils from BM, the open-chest procedure per se initiated hallmark features of
323 emergency granulopoiesis. These included sustained elevations of the cytokines (G-CSF and
324 CXCL1), a pronounced degenerative left shift with up to 80% immature neutrophils in
325 circulation, prolonged mobilization of immature cells beyond 72 hours, and persistent
326 alterations in the BM requiring more than a week for recovery. This is in agreement with
327 earlier studies showing that surgical procedures in cardiovascular disease models alter
328 myeloid cell populations[30], including the induction of robust neutrophil mobilization[31]. It
329 should be noted that signs of emergency granulopoiesis have been observed in previous MI
330 studies[32], however the contribution of the surgical procedure itself to this response had not
331 been evaluated. Collectively, our findings reveal a major translational challenge, as surgical
332 trauma inherent to the open-chest model induces systemic inflammation that masks disease-
333 specific immune responses.

334 By contrast, we found that the minimally invasive intact-chest model provides a more
335 pathophysiologically relevant alternative. In this setting, MI itself elicited only an acute and
336 mild inflammatory response, characterized by transient cytokine elevation, preserved BM
337 homeostasis, and a modest left shift that closely mirrored the neutrophil profile observed in
338 human MI patients[23] (Fig. 1). In this context, the MI-induced left shift most likely resulted from

339 rapid mobilization of BM reserves rather than emergency granulopoiesis. Consequently,
340 interventions targeting emergency granulopoiesis may be ineffective against the physiological
341 mobilization that occurs in actual MI. This may explain the frequent failure of anti-
342 inflammatory therapies that appear promising in preclinical studies using conventional open-
343 chest models[8,33,34].

344 To clarify post-MI neutrophil dynamics, especially immature neutrophil mobilization, we
345 examined the spatiotemporal sequence of events following ischemia. We observed an early
346 peak of neutrophil-mobilizing cytokines (G-CSF and IL-6) at 4 hours post-MI, followed by BM
347 neutrophils egress at 12 hours, resulting in a marked rise in circulating immature neutrophils
348 (≈ 32% of total neutrophils). This pattern closely aligns with previous findings from Ulrich *et*
349 *al*.[17], showing that a single G-CSF injection causes rapid mobilization of immature neutrophils,
350 peaking at 12 hours at 28% of total neutrophils. The similarity in both timing and magnitude,
351 between Ulrich's study and our MI data, strongly suggests that G-CSF is the main driver of
352 immature neutrophil release from the M after MI. Mechanistically, G-CSF is known to disrupt
353 the CXCL12–CXCR4 retention axis in the BM, thereby promoting neutrophil egress[35]. IL-6 was
354 also shown to mobilize immature neutrophils[36], albeit more modestly (≈ 8% at 12 hours).
355 Given that cytokines can act additively[37,38], the simultaneous rise of G-CSF and IL-6 after MI
356 likely explains the rapid, transient release of immature neutrophils. Additionally, we observed
357 a rapid increase in plasma CXCL1 post-MI which may contribute to immature neutrophil
358 release as CXCL1 has been shown to cooperate with G-CSF in neutrophil mobilization[39].
359 Together, these findings indicate that myocardial ischemia alone generates a moderate
360 inflammatory stimulus that primarily mobilizes pre-existing bone marrow neutrophil pools,
361 rather than inducing emergency granulopoiesis.

362 Once released into the bloodstream, we found that immature neutrophils migrated to the
363 damaged myocardium as effectively as mature neutrophils with peak accumulation at 12-24
364 hours post-MI. Previous studies have demonstrated that immature neutrophils possess the
365 functional migratory machinery required to infiltrate tumors[15], we show here that they are
366 also capable of infiltrating ischemic cardiac tissue. To date, the best-established routes of
367 leukocyte entry into the infarcted heart include transmigration through the microvasculature
368 in the border zone and infiltration through adipose tissue connected to the epicardium[40-42].

369 Notably, a recent study using cutting-edge spatial multi-omics technologies with subcellular
370 resolution identified a previously unrecognized route of monocyte infiltration into the
371 infarcted myocardium via the endocardium[29]. Reanalysis of the antibody-based Sequential
372 Immunofluorescence dataset from this study revealed that neutrophils were localized not
373 only to the border zone and the region adjacent to the epicardium, but also beneath the
374 endocardial surface. This raises the possibility that neutrophils, like monocytes, may be
375 recruited through the endocardium. Further investigations will be required to delineate the
376 molecular pathways governing the distinct routes of neutrophil trafficking.
377
378 To specifically assess the functions of immature neutrophils post-MI, we enhanced their
379 mobilization using G-CSF/anti–G-CSF antibody complexes, which prolong G-CSF half-life and
380 enhance its biological activity[15,43]. We showed that, after MI, G-CSF treatment increased
381 immature neutrophil numbers in blood and proportionally in infarcted tissue. This
382 accumulation was associated with impaired cardiac function, larger infarcts, and pathological
383 remodeling. These results establish a causal role for immature neutrophils in maladaptive
384 remodeling. Importantly, this has direct clinical relevance as a recent study showed that
385 elevated circulating immature granulocytes in MI patients is associated with a more than 5–
386 6-fold increase in 30-day mortality risk[24]. Together, these findings highlight that immature
387 neutrophils are not mere bystanders but rather act as key mediators of post-infarct pathology
388 and may serve as valuable biomarkers for risk stratification and outcome prediction.
389
390 Neutrophils contribute to tissue repair by clearing dead cells, but their effector functions can
391 also cause collateral damage. A growing body of evidence suggests that immature neutrophils
392 play pathological roles in cancer[13,44] and their accumulation in tumors correlates with a poor
393 prognosis[15,45-47]. By contrast, far less is known about the role of immature neutrophils in non-
394 malignant diseases. While a previous study showed that resting immature neutrophils in the
395 BM had limited effector capacity[15], we demonstrated that immature neutrophils infiltrating
396 the infarcted myocardium are functionally competent cells. Indeed, cardiac immature
397 neutrophils mounted a robust oxidative burst, comparable to mature neutrophils and
398 displayed phagocytic capacity. We propose here two non-mutually exclusive explanations for
399 the observed pathological consequences on the infarcted heart associated with immature
400 neutrophil accumulation. First, and most importantly, we would expect a higher number of

401 competent neutrophils, regardless of maturation state, to exarcebate the overall
402 inflammatory response. An excess of ROS-producing cells should increase oxidative stress on
403 cardiomyocytes, endothelial cells, and extracellular matrix, thereby amplifying tissue
404 injury[48,49]. Second, although marginal, we observed a reduced phagocytic capacity in
405 immature neutrophils compared to mature neutrophils, which may limit to some extent the
406 efficiency of efferocytosis, a process essential for clearing apoptotic cells and resolving
407 inflammation. Inadequate debris clearance promotes the persistence of pro-inflammatory
408 signals[50], consistent with the elevated IL-6 levels we observed at 28 days post-MI. Notably, a
409 comparable neutrophil phenotype has been described in the inflammatory vascular disease
410 giant cell arteritis[51], where immature neutrophils were similarly shown to produce high levels
411 of ROS, comparable to mature neutrophils, while exhibiting a modestly reduced phagocytic
412 capacity, and where their accumulation was associated with increased tissue damage and
413 vascular pathology. Taken together, we propose that the higher number of total ROS-
414 competent neutrophils (comprised from both mature and immature neutrophils) in the
415 infarcted heart, combined with suboptimal clearance by immature neutrophils, sustains local
416 inflammation, exacerbates tissue injury, and ultimately impairs cardiac healing and function.
417
418 Beyond neutrophils, the intact-chest MI model revealed distinct patterns of immune cell
419 recruitment that differ in magnitude, kinetics, and composition compared with the open-
420 chest model, suggesting that previous studies may have mischaracterized some aspects of the
421 inflammatory response following MI[2-4,52]. For instance, we found that the accumulation of T
422 cells, B cells, and neutrophils in the heart was markedly higher in the open-chest model,
423 indicating that surgical trauma in the open-chest model induces a strong ischemia-
424 independent inflammatory response. We also observed divergent profiles of monocytes,
425 macrophages, and CD11c^{+} cells between the two models. Further work will be required to
426 delineate the molecular pathways underlying these model-specific differences and to define
427 the precise roles of individual immune-cell subsets in the intact-chest MI model.
428
429 In conclusion, our study underscores the importance of using pathophysiologically accurate
430 experimental models. As George E. P. Box famously noted: "All models are wrong, but some
431 are useful"[53]. The careful selection of models and controls has become increasingly
432 recognized as essential for correctly defining the cellular and molecular pathways involved in

433 cardiovascular disease[54-56]. Building upon the technical foundation established by Sicklinger
434 and colleagues[28], our findings demonstrate that the intact-chest MI model represents the
435 more useful choice with respect to immune response characterization as it avoids the
436 confounding effects of surgical trauma. Using neutrophils as a benchmark, we showed that
437 the murine intact-chest MI model faithfully recapitulates human neutrophil responses in AMI
438 patients and revealed the pathogenic contribution of immature neutrophils to heart failure.
439 Although our study focused primarily on neutrophils, our findings also suggest that the ic-MI
440 model may better reflect aspects of the broader post-MI immune landscape. We anticipate
441 that future studies using the intact-chest MI model will clarify the roles of the different
442 immune cell types in disease progression with higher clinical relevance and facilitate the
443 identification of therapeutic targets specifically addressing the pathophysiological
444 inflammatory processes of MI.

445 **Methods**

446 **Ethics declarations**

447 All experiments involving human specimens were approved by the research ethics
448 committees of the National Healthcare Group Domain Specific Review Board (NHG DSRB
449 Domain C 2020/01253). All procedures involving animals were performed conform to the
450 guidelines from Directive 2010/63/EU, the government of Upper Bavaria ((ROB-
451 55.2.2532.Vet_02-13-176, 55.2.2532.Vet_02-18-114 and 55.2.2532.Vet_23-157), Germany,
452 and the Institutional Animal Care and USA Committee (IACUC), in accordance with the
453 guidelines of the Agri-Food and Veterinary Authority (AVA) and the National Advisory
454 Committee for Laboratory Animal Research (NACLAR) of Singapore. All procedures had local
455 ethical approval, and all experiments were conducted according to the 2013 Declaration of
456 Helsinki.

457

458 **Human data and study design**

459 Among twenty patients with acute myocardial infarction (AMI), 13 met the inclusion criteria
460 and were categorized into non-ST-elevation MI (NSTEMI) and ST-elevation MI (STEMI). All
461 details regarding the patients are provided in **Supplementary Table 1**. Five healthy donors
462 (HD) were recruited as control subjects.

463

464 **Flow cytometry of human blood samples**

465 Venous blood was collected in EDTA tubes. For multiparameter flow cytometry, 2mL of whole
466 blood were lysed using 20 mL of 1X RBC lysis buffer (eBioscience) for 6 min at room
467 temperature. The lysis reaction was stopped by adding 30 mL of PBS, and cells were
468 centrifuged at 400 g for 5 min. RBC lysis step was repeated once. Subsequently cells were
469 blocked with anti-human CD32 antibody for 15 min, followed by fluorochrome-conjugated
470 antibodies (**Supplementary Table 2**) for 30 min at 4 °C. Cells were washed, resuspended in
471 PBS containing DAPI, and data was acquired on a LSRII flow cytometer (BD Biosciences).
472 Analysis of immune cell populations and applied gating strategies were conducted with
473 FlowJo software (v10.8.0, TreeStar). Neutrophils were defined as $CD45^+$ Lin^- $CD15^+$ $CD66b^+$
474 $CD49d^-$ $CD11b^+$. CD16 and CD10 expression was used to distinguish mature ($CD16^+$ $CD10^+$)

475 and immature ($CD16^{+/-}$ $CD10^{-}$) neutrophils. Representative gating strategy is shown in
476 **Extended Data Figure 1**.
477
478 **Mouse experiments**
479 Female C57BL/6J mice (9-12 weeks old; Janvier Labs) were housed under standard laboratory
480 conditions with a 12-hour light/dark cycle and provided chow and water ad libitum. Animals
481 were subjected to either sham-operation (SO) or myocardial infarction (MI). Healthy
482 untouched mice were used as baseline controls (BL). All surgeries were performed between
483 ZT3 and ZT5 to prevent circadian rhythm influencing neutrophil dynamics on time of surgery.
484
485 **Open-chest MI model**
486 In the open-chest (oc) model, MI was induced via invasive surgery and permanent ligation of
487 the left anterior descending coronary artery (LAD) as described previously[9,57]. In brief, mice
488 were anesthetized with midazolam (5 mg/kg), medetomidine (0.5 mg/kg), and fentanyl (0.05
489 mg/kg), followed by endotracheal intubation and ventilation using a MiniVent ventilator
490 (Harvard Apparatus, Holliston, MA). Thoracotomy was performed on the left side at the third
491 intercostal space, the pericardium was opened, and the LAD was permanently ligated
492 proximal to its bifurcation using 7-0 permahand silk threads (Ethicon, Somerville, USA). The
493 intercostal space and skin were closed with 5-0 Seraflex silk (Serag Wiessner, Germany).
494 Anesthesia was reversed with flumazenil (0.5 mg/kg), and atipamezole (2.5 mg/kg). Analgesia
495 (buprenorphine, 0.05 mg/kg) was administered 30 min pre as well as 6 and 18 h post-surgery.
496 Sham-operated (oc-SO) animals underwent the same procedure without LAD ligation.
497
498 **Intact-chest MI model**
499 In the intact-chest (ic) model, minimally invasive MI induction was performed under
500 echocardiographic guidance as described by Sicklinger et al[28]. In brief, mice were anesthetized
501 with isoflurane (1 L O_2/min; 3-4% for induction and 1-2% for procedure) and positioned on a
502 Vevo imaging station (Vevo3100, VisualSonics Inc,). The LAD coronary artery was visualized at
503 the mid-papillary level using Color Doppler imaging. A monopolar needle attached to a
504 micromanipulator was introduced through the chest and placed directly onto the LAD. Artery
505 vessel was coagulated with high-frequency electricity (HF-Gerät Erbe ICC 200). Successful MI
506 induction was confirmed by persistent loss of Doppler flow and akinesia of the affected left

507 ventricular region. Analgesia (buprenorphine, 0.1 mg/kg) was administered 30 min pre and 6
508 h post-surgery. Sham-operated (ic-SO) animals underwent the same procedure without
509 electrical coagulation.
510
511 **Organ collection and processing**
512 Animals were euthanized with ketamine/xylazine overdose (*i.p.*; 150/30 mg/kg) at respective
513 time points post-MI (4h, 12h, 24h, 72h, 5d, 7d). Whole blood was collected via cardiac
514 puncture in EDTA-coated tubes. After transcardiac perfusion with ice-cold PBS to remove
515 remaining blood within the heart and vessels, the following organs: tibia, femur, spleen,
516 mediastinal lymph nodes (MLNs), peripheral lymph nodes (axillary and inguinal; LN), left lung
517 lobe and hearts (without atria) were excised and further processed. Tibia length was
518 measured to normalize heart weight.
519
520 **Flow cytometry**
521 Cardiac tissues were minced with fine scissors and digested with Collagenase Type I (450
522 U/mL), Collagenase Type XI (125 U/mL), DNase I (60 U/mL) and Hyaluronidase (60 U/mL) for
523 1h at 37°C. Bone marrow (BM) cells were isolated from one femur by removing the epiphysis
524 and centrifuging for 2 min at 10'000 rpm. Lungs were minced with fine scissors and digested
525 with Collagenase Type I (450 U/mL), Hyaluronidase (120 U/mL), and DNase I (240 U/mL) for
526 45min at 37 °C. Spleens, MLN and peripheral LNs were mashed through a 50 µm filter. Red
527 blood cells in blood, spleen and lung were lysed using RBC lysis buffer (BioLegend). All cells
528 were washed and resuspended in FACS Buffer (PBS containing 1% BSA). Fc receptors were
529 blocked with rat anti-mouse CD16/32 antibody (clone 93, BioLegend) and surface proteins
530 stained for 45 min at 4°C with antibodies (**Supplementary Table 2).** Following washing, cells
531 were resuspended in FACS Buffer containing CountBright Absolute Counting Beads (Life
532 Technologies) and measured with an LSRFortessa X-20 flow cytometer (BD Biosciences).
533 Analysis of immune cell populations and applied gating strategies were conducted with
534 FlowJo software (v10.8.0, TreeStar). Neutrophils were defined as $CD45^+$ $CD11b^+$ $CD115^-$ $Ly6G^+$
535 in blood, $Lineage^-$ $CD45^+$ $CD11b^+$ $CD115^-$ $Ly6G^+$ in bone marrow, and $CD45^+$ $CD11b^+$ $Ly6G^+$ in
536 the heart. CD101 expression was used to distinguish mature ($CD101^+$) and immature ($CD101^-$)
537 neutrophils. A CD101 fluorescence minus one (FMO) control was included to accurately define
538 positive and negative populations. Representative gating strategies and FMO stainings are

539 shown in **Extended Data Figures 2 and 5**. CXCR2 expression in BM immature neutrophils was
540 quantified as geometric mean fluorescence intensity (MFI). For comparative analysis, MFI
541 values from BM cells of oc-SO, oc-MI, ic-SO, and ic-MI groups were normalized to the MFI of
542 the respective marker in immature neutrophils from the baseline (BL) group.
543
544 **ROS production and phagocytosis assay**
545 Reactive oxygen species (ROS) production was quantified by incubating cells with 5 µM
546 Dihydrorhodamine 123 (DHR 123, Sigma-Aldrich) for 10 min at 37°C. Oxidation of DHR to
547 fluorescent rhodamine 123 was measured by flow cytometry (FITC channel). Phagocytic
548 activity was assessed using pHrodo™ Deep Red *E. coli* BioParticles™ (Invitrogen). Cells were
549 incubated with 40 µg of opsonized BioParticles for 30 min at 37°C. Upon internalization into
550 acidic phagosomes, pHrodo fluorescence increases, allowing quantification of phagocytosis
551 by flow cytometry (Deep Red channel). Following incubation, cells were washed with FACS
552 buffer and stained with fluorochrome-conjugated antibodies as described above. After a final
553 wash, cells were resuspended in FACS buffer and acquired on an LSRFortessa X-20 flow
554 cytometer (BD Biosciences). Data were analyzed using FlowJo software (v10.8.0, TreeStar).
555
556 **Increased immature neutrophils recruitment via G-CSF injection**
557 To increase circulating immature neutrophil counts, mice were treated with G-CSF/anti–G-
558 CSF antibody complexes, which prolong G-CSF half-life and enhance its biological activity, as
559 previously described by Rubinstein et al.[43] and Evrard et al.[15]. Briefly, human G-CSF
560 (PeproTech) was incubated with rat anti-human G-CSF antibody (clone BVD11-37G10,
561 Southern Biotech) at a 1:6 ratio for 20 min at 37 °C. The resulting complex was diluted in
562 sterile PBS to a final dose of 1.5 µg G-CSF in 100 µL per mouse. Mice received a single
563 intraperitoneal injection of the complex or vehicle (PBS) immediately after MI induction in
564 the intact-chest model. Tissues were harvested 24h or 28 days post-MI, as described above.
565
566 **Cytokine and chemokine immunoassays**
567 Plasma was collected by centrifuging blood for 10 min at 10’000 rpm. Cytokine and chemokine
568 levels were assessed using a custom-made ProcartaPlex (ThermoFisher) containing
569 GROα/CXCL1, MCP-1/CCL2, G-CSF, IL-6, and TNFα, as well as DuoSet ELISAs for mouse CXCL1,
570 G-CSF, and IL-6 (R&D Systems) following manufacturers’ protocols.

571 **Gene expression analysis**

572 Cardiac apex and base of G-CSF and PBS injected mice (28d post-MI) were snap frozen. Frozen
573 hearts were first pestilled in liquid nitrogen to a fine powder, then lysed in RLT Plus buffer
574 (Qiagen) supplemented with β-mercaptoethanol and homogenized using a bead mill (Ø7mm).
575 RNA was isolated with RNeasy Plus Micro Kit (Qiagen) following manufacturer's protocol.
576 Using the PrimeScript RT Reagent Kit (TaKaRa Bio), 1 µg of RNA was reverse transcribed and
577 25 ng of the resulting cDNA per reaction was used for TaqMan real-time RT-PCR analysis.
578 mRNA expression was determined for *Nppa* (Mm01255747_g1), *Myh6* (Mm00440359_m1),
579 *Myh7* (Mm00600555_m1) and *Il6* (Mm00446190_m1) (Applied Biosystems). Samples were
580 run in duplicates using a QuantStudio 6 Pro Real-Time-PCR-System (ThermoFisher) and mRNA
581 expression was normalized to *Gapdh* levels (Mm99999915_g1, Applied Biosystems). Relative
582 gene expression was calculated with the comparative ΔΔCT method.

583

584 **Histology**

585 Mid-section of hearts from G-CSF and PBS injected mice (28d post-MI) were embedded in
586 Tissue-Tek Optimal Cutting Temperature (O.C.T) compound in a plastic cassette and were
587 immediately snap frozen. Hearts were stored at -80 °C and further sectioned at 5µm thickness
588 using a Leica CM3050S cryostat. Tissue sections were stained with a Masson's Trichrome
589 (Sigma-Aldrich) according to the manufacturer's instructions. Brightfield images were
590 acquired using a Leica Thunder microscope (Leica Microsystems) and analyzed with
591 Fiji/ImageJ (https://imagej.net). For each data point, three sections from the apex, mid, and
592 proximal infarct area were analyzed and averaged**.** Scar size measurement: scarred regions
593 were manually delineated based on blue collagen staining, measured, and normalized to the
594 total left ventricular area. Fibrosis content measurement: fibrosis was quantified as the
595 proportion of collagen-positive tissue relative to the total left ventricular area. The left
596 ventricle was manually outlined to define the total ventricular area, and blue-stained collagen
597 was isolated using color thresholding (Chanel_1 in Colour Deconvolution plugin).

598

599 **Echocardiography**

600 Echocardiographic scans of the parasternal long axis were obtained 28 days post-MI from
601 mice treated with G-CSF or PBS using the Vevo 3100 imaging system (VisualSonics Inc.). Mice
602 were anesthetized with isoflurane (3-4% for induction and 1-2% for acquiring scans) at a flow

603 rate of 1L O_2/min. Heart rate and body temperature were kept stable throughout the
604 procedure. Left ventricular end-diastolic volume, end-systolic volume and ejection fraction
605 were measured based on the left parasternal long-axis view using VevoLab software version
606 5.10.0 (VisualSonics). Global longitudinal strain was quantified in the longitudinal axis by
607 speckle tracking using VevoStrain.
608
609 **Mapping of neutrophils in cardiac tissue**
610 To assess the spatial distribution of neutrophils within infarcted cardiac tissue, we analyzed
611 data from the open-source SeqIF dataset generated by Wünnemann et al.[29]. In that study,
612 cryosections (8 µm) of mouse hearts collected 24 h after intact-chest MI were stained with a
613 12-antibody panel using the Lunaphore COMET platform (Lunaphore Technologies). We
614 downloaded the raw TIFF files from Synapse (https://www.synapse.org, accession:
615 syn51449058) and high-resolution images (30,238 × 28,381 pixels) containing MPO**,** Tnnt2**,**
616 and Ankrd1 staining were selected and processed using Fiji/ImageJ.
617
618 **Statistical Analysis**
619 After performing a normality test, an unpaired Welch's *t*-test or Mann-Whitney test was
620 performed for comparisons between two groups. For comparisons within three groups, a one-
621 way ANOVA followed by Bonferroni's *post hoc* was performed. For comparisons within two
622 or more groups within different time points, a two-way ANOVA with Šidák's or Tukey's *post*
623 *hoc* if appropriate was used. Paired or unpaired multiple *t*-tests with Holm–Šidák's correction
624 were used for comparisons between ic-SO and ic-MI groups. All details of the statistical tests
625 used are provided in the figure legends. Statistical significance is represented by asterisks and
626 the corresponding *p* values, as indicated in the legends. Data are expressed as mean ± SEM.
627 Biological replicates are stated in the legends for each figure. All statistical analysis were
628 performed with Prism10 (v10.4.1, GraphPad). Heat maps were created with Morpheus
629 analysis software (https://software.broadinstitute.org/morpheus).
630

Acknowledgments

We acknowledge the support by Deutsche Forschungsgemeinschaft (DFG) (SFB1123-A1/A10 to J.D. and C.W., SFB1123-B09, STE1053/5-1, STE1053/8-1 to S.S.), by the German Center for Cardiovascular Research (DZHK) (81X2600271, 81X2600275 and 81X2600283 to J.D., 1X2600254 to C.W. and 81Z0600205 to S.S.), by Förderprogramm für Forschung und Lehre (FöFoLe) (68/2013 to S.S). I.K. was supported by the Singapore Immunology Network (SIgN) Agency for Science, Technology and Research (A*STAR).

Author contributions

Z.M.R. and A.K. designed experiments, performed mouse experiments, flow cytometry experiments and echocardiography measurements, analyzed data, and contributed to writing the manuscript. S.L.P. and M.S. performed mouse experiments and analyzed data. Y.J. performed tissue embedding/sectioning. A.E. performed gene expression experiments. K.N. performed flow cytometry experiments and analyzed data. I.K. and M.Y.Y.C. provided and analyzed data from human AMI samples and provided intellectual input. F.S. and F.L. provided assistance with intact-chest mouse model and provided intellectual input. C.W. provided intellectual input and funding. S.S. provided strategic input and funding, obtained animal experimentation approvals and supervised research enabling the implementation of MI mouse models. J.D. designed and supervised the study, planned experiments, provided funding, and wrote the manuscript with input from all authors.

651 **References**

652 1. Khan MA, Hashim MJ, Mustafa H, et al. Global Epidemiology of Ischemic Heart Disease: Results
653 from the Global Burden of Disease Study. *Cureus*. Jul 23 2020;12(7):e9349. doi:10.7759/cureus.9349
654 2. Ong SB, Hernandez-Resendiz S, Crespo-Avilan GE, et al. Inflammation following acute myocardial
655 infarction: Multiple players, dynamic roles, and novel therapeutic opportunities. *Pharmacol Ther*. Jun
656 2018;186:73-87. doi:10.1016/j.pharmthera.2018.01.001
657 3. Kologrivova I, Shtatolkina M, Suslova T, Ryabov V. Cells of the Immune System in Cardiac
658 Remodeling: Main Players in Resolution of Inflammation and Repair After Myocardial Infarction. *Front*
659 *Immunol*. 2021;12:664457. doi:10.3389/fimmu.2021.664457
660 4. Yan X, Anzai A, Katsumata Y, et al. Temporal dynamics of cardiac immune cell accumulation
661 following acute myocardial infarction. *J Mol Cell Cardiol*. Sep 2013;62:24-35.
662 doi:10.1016/j.yjmcc.2013.04.023
663 5. Chia S, Nagurney JT, Brown DF, et al. Association of leukocyte and neutrophil counts with infarct
664 size, left ventricular function and outcomes after percutaneous coronary intervention for ST-elevation
665 myocardial infarction. *Am J Cardiol*. Feb 1 2009;103(3):333-7. doi:10.1016/j.amjcard.2008.09.085
666 6. Meissner J, Irfan A, Twerenbold R, et al. Use of neutrophil count in early diagnosis and risk
667 stratification of AMI. *Am J Med*. Jun 2011;124(6):534-42. doi:10.1016/j.amjmed.2010.10.023
668 7. Puhl SL, Steffens S. Neutrophils in Post-myocardial Infarction Inflammation: Damage vs.
669 Resolution? *Front Cardiovasc Med*. 2019;6:25. doi:10.3389/fcvm.2019.00025
670 8. Vinten-Johansen J. Involvement of neutrophils in the pathogenesis of lethal myocardial
671 reperfusion injury. *Cardiovasc Res*. Feb 15 2004;61(3):481-97. doi:10.1016/j.cardiores.2003.10.011
672 9. Horckmans M, Ring L, Duchene J, et al. Neutrophils orchestrate post-myocardial infarction healing
673 by polarizing macrophages towards a reparative phenotype. *Eur Heart J*. Jan 14 2017;38(3):187-197.
674 doi:10.1093/eurheartj/ehw002
675 10. Ma Y, Yabluchanskiy A, Lindsey ML. Neutrophil roles in left ventricular remodeling following
676 myocardial infarction. *Fibrogenesis Tissue Repair*. Jun 3 2013;6(1):11. doi:10.1186/1755-1536-6-11
677 11. Akpek M, Kaya MG, Lam YY, et al. Relation of neutrophil/lymphocyte ratio to coronary flow to in-
678 hospital major adverse cardiac events in patients with ST-elevated myocardial infarction undergoing
679 primary coronary intervention. *Am J Cardiol*. Sep 1 2012;110(5):621-7. doi:10.1016/j.amjcard.2012.04.041
680 12. Vafadarnejad E, Rizzo G, Krampert L, et al. Dynamics of Cardiac Neutrophil Diversity in Murine
681 Myocardial Infarction. *Circ Res*. Oct 9 2020;127(9):e232-e249. doi:10.1161/CIRCRESAHA.120.317200
682 13. Ng LG, Ostuni R, Hidalgo A. Heterogeneity of neutrophils. *Nat Rev Immunol*. Apr 2019;19(4):255-
683 265. doi:10.1038/s41577-019-0141-8
684 14. Kwok I, Becht E, Xia Y, et al. Combinatorial Single-Cell Analyses of Granulocyte-Monocyte
685 Progenitor Heterogeneity Reveals an Early Uni-potent Neutrophil Progenitor. *Immunity*. Aug 18
686 2020;53(2):303-318 e5. doi:10.1016/j.immuni.2020.06.005
687 15. Evrard M, Kwok IWH, Chong SZ, et al. Developmental Analysis of Bone Marrow Neutrophils Reveals
688 Populations Specialized in Expansion, Trafficking, and Effector Functions. *Immunity*. Feb 20 2018;48(2):364-
689 379 e8. doi:10.1016/j.immuni.2018.02.002
690 16. Nauseef WM, Borregaard N. Neutrophils at work. *Nat Immunol*. Jul 2014;15(7):602-11.
691 doi:10.1038/ni.2921
692 17. Ulich TR, del Castillo J, Souza L. Kinetics and mechanisms of recombinant human granulocyte-
693 colony stimulating factor-induced neutrophilia. *Am J Pathol*. Dec 1988;133(3):630-8.
694 18. Pietras EM, Mirantes-Barbeito C, Fong S, et al. Chronic interleukin-1 exposure drives
695 haematopoietic stem cells towards precocious myeloid differentiation at the expense of self-renewal. *Nat*
696 *Cell Biol*. Jun 2016;18(6):607-18. doi:10.1038/ncb3346
697 19. Boettcher S, Ziegler P, Schmid MA, et al. Cutting edge: LPS-induced emergency myelopoiesis
698 depends on TLR4-expressing nonhematopoietic cells. *J Immunol*. Jun 15 2012;188(12):5824-8.
699 doi:10.4049/jimmunol.1103253
700 20. Manz MG, Boettcher S. Emergency granulopoiesis. *Nat Rev Immunol*. May 2014;14(5):302-14.
701 doi:10.1038/nri3660
702 21. Boettcher S, Manz MG. Regulation of Inflammation- and Infection-Driven Hematopoiesis. *Trends*
703 *Immunol*. May 2017;38(5):345-357. doi:10.1016/j.it.2017.01.004

22. Yvan-Charvet L, Ng LG. Granulopoiesis and Neutrophil Homeostasis: A Metabolic, Daily Balancing Act. *Trends Immunol*. Jul 2019;40(7):598-612. doi:10.1016/j.it.2019.05.004

23. Fraccarollo D, Neuser J, Moller J, Riehle C, Galuppo P, Bauersachs J. Expansion of CD10(neg) neutrophils and CD14(+)HLA-DR(neg/low) monocytes driving proinflammatory responses in patients with acute myocardial infarction. *Elife*. Jul 22 2021;10doi:10.7554/eLife.66808

24. Richter M, von Göwels J, Fähndrich M, et al. Neutrophil progenitor mobilization is a distinct feature of STEMI and predicts survival. Preprint. *Research Square*. 2025;doi:10.21203/rs.3.rs-6474581/v2

25. De Villiers C, Riley PR. Mouse models of myocardial infarction: comparing permanent ligation and ischaemia-reperfusion. *Dis Model Mech*. Nov 18 2020;13(11)doi:10.1242/dmm.046565

26. Johns TN, Olson BJ. Experimental myocardial infarction. I. A method of coronary occlusion in small animals. *Ann Surg*. Nov 1954;140(5):675-82. doi:10.1097/00000658-195411000-00006

27. Lindsey ML, Bolli R, Canty JM, Jr., et al. Guidelines for experimental models of myocardial ischemia and infarction. *Am J Physiol Heart Circ Physiol*. Apr 1 2018;314(4):H812-H838. doi:10.1152/ajpheart.00335.2017

28. Sicklinger F, Zhang Y, Lavine KJ, et al. A Minimal-Invasive Approach for Standardized Induction of Myocardial Infarction in Mice. *Circ Res*. Oct 9 2020;127(9):1214-1216. doi:10.1161/CIRCRESAHA.120.317794

29. Wunnemann F, Sicklinger F, Bestak K, et al. Spatial multiomics of acute myocardial infarction reveals immune cell infiltration through the endocardium. *Nat Cardiovasc Res*. Oct 2025;4(10):1345-1362. doi:10.1038/s44161-025-00717-y

30. Hoffmann J, Ospelt M, Troidl C, et al. Sham surgery and inter-individual heterogeneity are major determinants of monocyte subset kinetics in a mouse model of myocardial infarction. *PLoS One*. 2014;9(6):e98456. doi:10.1371/journal.pone.0098456

31. Denes A, McColl BW, Leow-Dyke SF, et al. Experimental stroke-induced changes in the bone marrow reveal complex regulation of leukocyte responses. *J Cereb Blood Flow Metab*. Apr 2011;31(4):1036-50. doi:10.1038/jcbfm.2010.198

32. Sreejit G, Abdel-Latif A, Athmanathan B, et al. Neutrophil-Derived S100A8/A9 Amplify Granulopoiesis After Myocardial Infarction. *Circulation*. Mar 31 2020;141(13):1080-1094. doi:10.1161/CIRCULATIONAHA.119.043833

33. Huang S, Frangogiannis NG. Anti-inflammatory therapies in myocardial infarction: failures, hopes and challenges. *Br J Pharmacol*. May 2018;175(9):1377-1400. doi:10.1111/bph.14155

34. Matter MA, Paneni F, Libby P, et al. Inflammation in acute myocardial infarction: the good, the bad and the ugly. *Eur Heart J*. Jan 7 2024;45(2):89-103. doi:10.1093/eurheartj/ehad486

35. Semerad CL, Liu F, Gregory AD, Stumpf K, Link DC. G-CSF is an essential regulator of neutrophil trafficking from the bone marrow to the blood. *Immunity*. Oct 2002;17(4):413-23. doi:10.1016/s1074-7613(02)00424-7

36. Suwa T, Hogg JC, English D, Van Eeden SF. Interleukin-6 induces demargination of intravascular neutrophils and shortens their transit in marrow. *Am J Physiol Heart Circ Physiol*. Dec 2000;279(6):H2954-60. doi:10.1152/ajpheart.2000.279.6.H2954

37. Ulich TR, del Castillo J, Busser K, Guo KZ, Yin SM. Acute in vivo effects of IL-3 alone and in combination with IL-6 on the blood cells of the circulation and bone marrow. *Am J Pathol*. Oct 1989;135(4):663-70.

38. Ulich TR, Yi ES, Yin S, et al. Hematologic effects of stem cell factor alone and in combination with G-CSF and GM-CSF in vivo and in vitro in rodents. *Int Rev Exp Pathol*. 1993;34 Pt A:215-33.

39. Wengner AM, Pitchford SC, Furze RC, Rankin SM. The coordinated action of G-CSF and ELR + CXC chemokines in neutrophil mobilization during acute inflammation. *Blood*. Jan 1 2008;111(1):42-9. doi:10.1182/blood-2007-07-099648

40. Horckmans M, Bianchini M, Santovito D, et al. Pericardial Adipose Tissue Regulates Granulopoiesis, Fibrosis, and Cardiac Function After Myocardial Infarction. *Circulation*. Feb 27 2018;137(9):948-960. doi:10.1161/CIRCULATIONAHA.117.028833

41. Swirski FK, Nahrendorf M. Cardioimmunology: the immune system in cardiac homeostasis and disease. *Nat Rev Immunol*. Dec 2018;18(12):733-744. doi:10.1038/s41577-018-0065-8

42. van der Laan AM, Ter Horst EN, Delewi R, et al. Monocyte subset accumulation in the human heart following acute myocardial infarction and the role of the spleen as monocyte reservoir. *Eur Heart J*. Feb 2014;35(6):376-85. doi:10.1093/eurheartj/eht331

43. Rubinstein MP, Salem ML, Doedens AL, et al. G-CSF/anti-G-CSF antibody complexes drive the potent recovery and expansion of CD11b+Gr-1+ myeloid cells without compromising CD8+ T cell immune responses. *J Hematol Oncol*. Oct 1 2013;6:75. doi:10.1186/1756-8722-6-75

44. Mackey JBG, Coffelt SB, Carlin LM. Neutrophil Maturity in Cancer. *Front Immunol*. 2019;10:1912. doi:10.3389/fimmu.2019.01912

45. Coffelt SB, Kersten K, Doornebal CW, et al. IL-17-producing gammadelta T cells and neutrophils conspire to promote breast cancer metastasis. *Nature*. Jun 18 2015;522(7556):345-348. doi:10.1038/nature14282

46. Sagiv JY, Michaeli J, Assi S, et al. Phenotypic diversity and plasticity in circulating neutrophil subpopulations in cancer. *Cell Rep*. Feb 3 2015;10(4):562-73. doi:10.1016/j.celrep.2014.12.039

47. Yang XD, Ai W, Asfaha S, et al. Histamine deficiency promotes inflammation-associated carcinogenesis through reduced myeloid maturation and accumulation of CD11b+Ly6G+ immature myeloid cells. *Nat Med*. Jan 2011;17(1):87-95. doi:10.1038/nm.2278

48. Moris D, Spartalis M, Tzatzaki E, et al. The role of reactive oxygen species in myocardial redox signaling and regulation. *Ann Transl Med*. Aug 2017;5(16):324. doi:10.21037/atm.2017.06.17

49. Hori M, Nishida K. Oxidative stress and left ventricular remodelling after myocardial infarction. *Cardiovasc Res*. Feb 15 2009;81(3):457-64. doi:10.1093/cvr/cvn335

50. Singh B, Li K, Cui K, et al. Defective efferocytosis of vascular cells in heart disease. *Front Cardiovasc Med*. 2022;9:1031293. doi:10.3389/fcvm.2022.1031293

51. Wang L, Ai Z, Khoyratty T, et al. ROS-producing immature neutrophils in giant cell arteritis are linked to vascular pathologies. *JCI Insight*. Oct 15 2020;5(20)doi:10.1172/jci.insight.139163

52. Nahrendorf M, Swirski FK, Aikawa E, et al. The healing myocardium sequentially mobilizes two monocyte subsets with divergent and complementary functions. *J Exp Med*. Nov 26 2007;204(12):3037-47. doi:10.1084/jem.20070885

53. Box GEP. *An accidental statistician : the life and memories of George E.P. Box*. John Wiley and Sons, Inc.,; 2013:1 online resource.

54. Rashbrook VS, Brash JT, Ruhrberg C. Cre toxicity in mouse models of cardiovascular physiology and disease. *Nat Cardiovasc Res*. Sep 2022;1:806-816. doi:10.1038/s44161-022-00125-6

55. Kass DA. Modeling HFpEF in animals. *Nat Cardiovasc Res*. Nov 28 2025;doi:10.1038/s44161-025-00754-7

56. Marks K, Ahn SJ, Rai N, Anfray A, Iadecola C, Anrather J. A minimally invasive thrombotic model to study stroke in awake mice. *Nat Commun*. May 10 2025;16(1):4356. doi:10.1038/s41467-025-59617-1

57. Puhl SL, Hilby M, Kohlhaas M, et al. Haematopoietic and cardiac GPR55 synchronize post-myocardial infarction remodelling. *Sci Rep*. Jul 13 2021;11(1):14385. doi:10.1038/s41598-021-93755-y

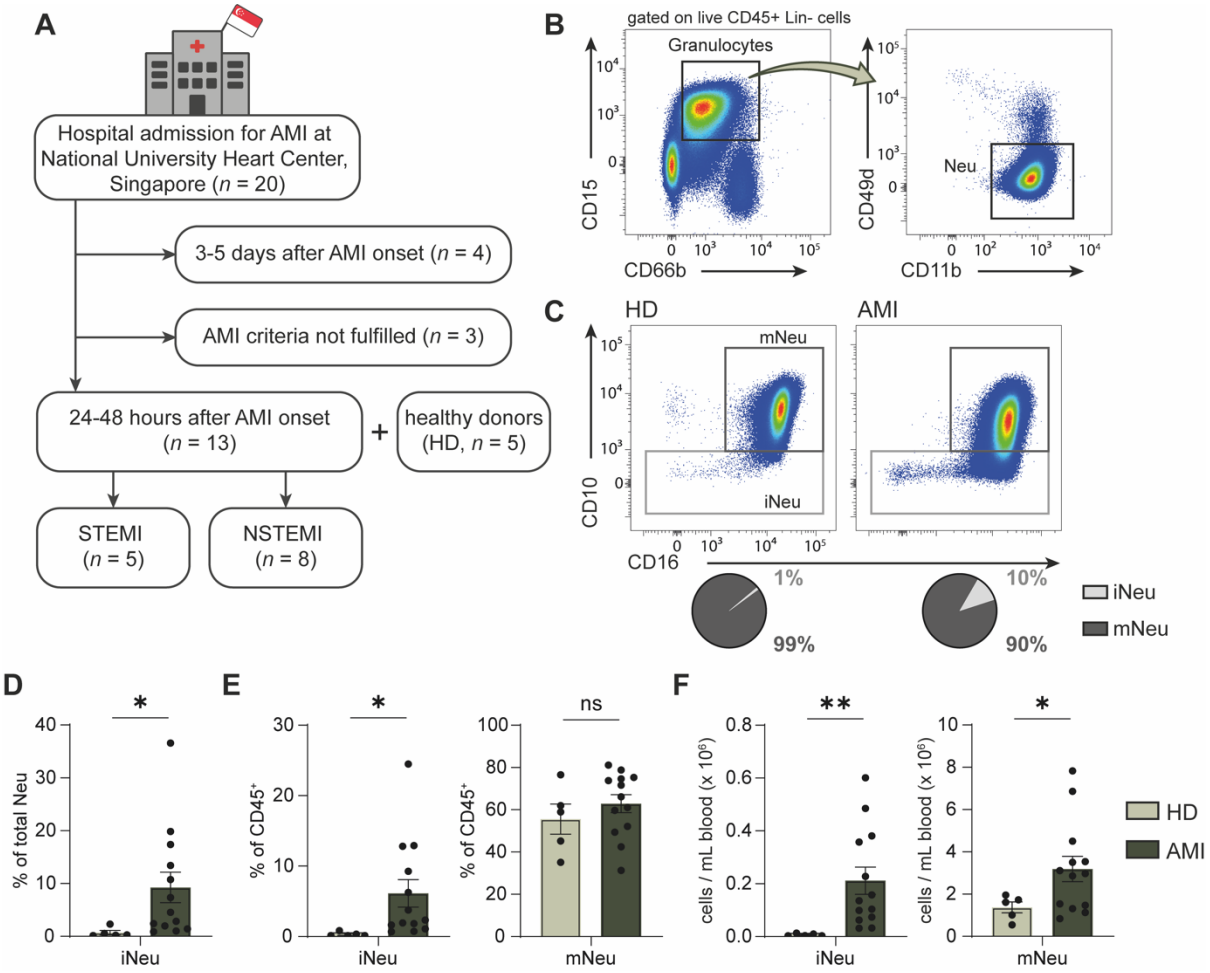

Figure 1. Presence of circulating immature neutrophils in AMI patients

(**A**) Schematic overview of the human study. Patients with acute myocardial infarction (AMI) were hospitalized at the National University Heart Center, Singapore (*n* = 20). Blood samples collected within 48h post-MI from patients (AMI, *n* = 13) and from healthy donors (HD, *n* = 5) were analyzed by flow cytometry. (**B**) Representative flow cytometry analysis to identify circulating neutrophils. Neutrophils were gated on the basis of CD45, CD15, CD66b and CD11b expression. Full gating strategy is available in Extended Data Fig. 1. (**C**) Representative flow cytometry analysis to distinguish neutrophil subsets based on CD10 expression in blood from donors (HD) and AMI patients. Pie charts represent the relative proportions of mature ($CD10^+$) and immature ($CD10^-$) subsets within total neutrophils. (**D**) Proportion of immature neutrophils within total circulating neutrophils. (**E**) Frequency of immature (left) and mature (right) neutrophils within $CD45^+$ white blood cells. (**F**) Absolute counts of immature (left) and mature (right) neutrophils. (**D-F**) Data are shown as mean ± SEM. Welch's *t*-test. *$p < 0.05$ and **$p < 0.01$. HD: $n = 5$; AMI: $n = 13$. ns, non-significant; STEMI, ST-elevated myocardial

808 infarction; NSTEMI, non-ST-elevated myocardial infarction; Neu, neutrophils; mNeu, mature
809 neutrophils; iNeu, immature neutrophils; Lin, Lineage (CD3, CD19, C56, CD14).
810
811

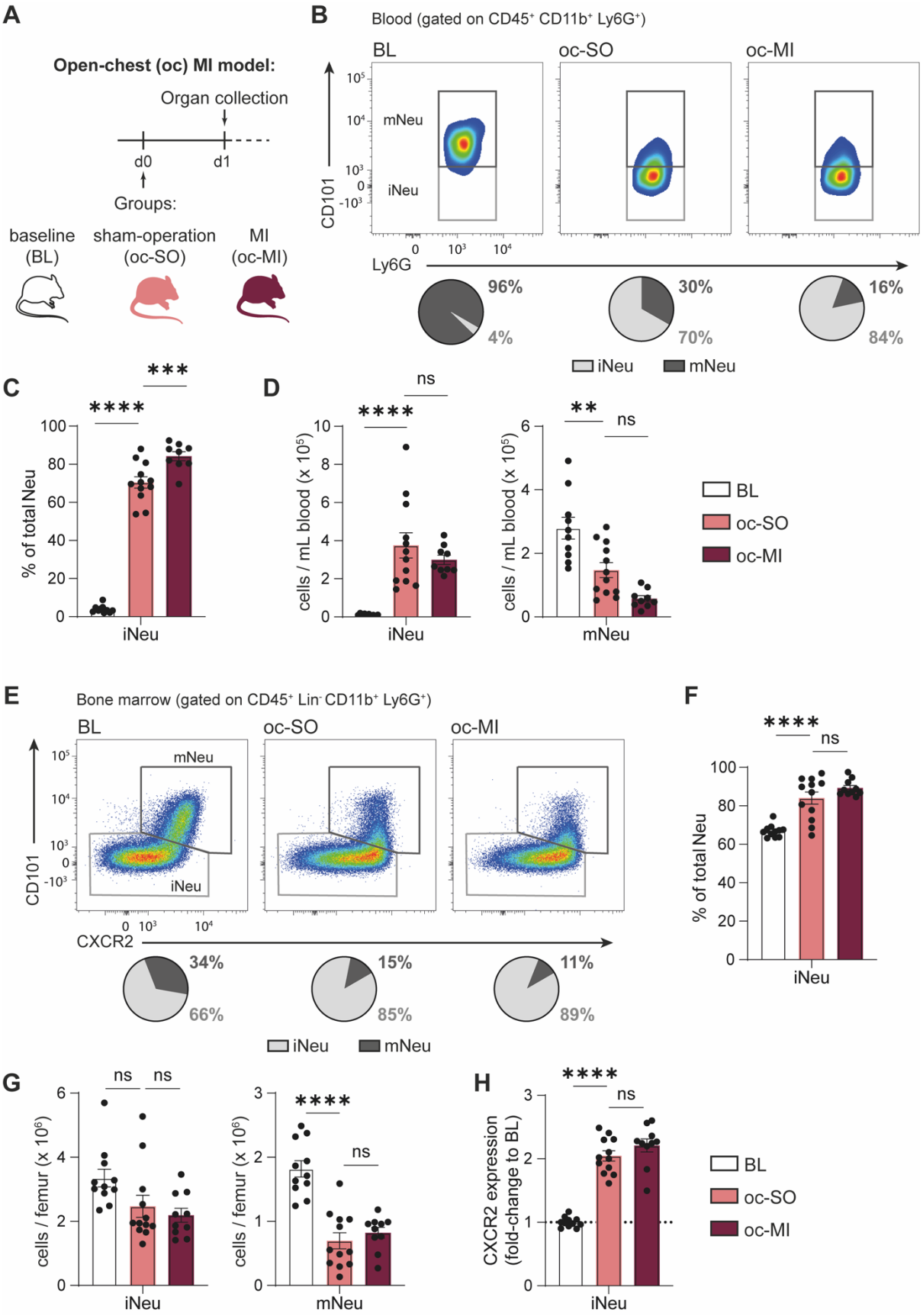

Figure 2. Surgery in open-chest MI model alters BM homeostasis and induces a marked increase in circulating immature neutrophils.

815 (**A**) Experimental design in the open-chest (oc) MI model: Mice were untreated as baseline
816 controls (BL, white), sham-operated (SO, light red), or subjected to LAD ligation (MI, dark red).
817 Blood and bone marrow (BM) were collected 24h post-intervention for flow cytometric
818 analysis. (**B**) Representative flow cytometry analysis to identify neutrophil subsets in blood.
819 $CD101^+$ neutrophils were classified as mature and $CD101^-$ as immature. Pie charts indicate the
820 average proportion of each subset within total circulating neutrophils. (**C-D)** Frequency of
821 immature neutrophils within total blood neutrophils (**C**) and absolute counts of circulating
822 immature (left) and mature (right) neutrophils (**D**). (**E**) Representative flow cytometry analysis
823 to identify neutrophil subsets in BM. $CD101^+$ neutrophils were considered mature, $CD101^-$
824 immature. Pie charts indicate the average proportion of each subset within total BM
825 neutrophils. (**F-G**) Frequency of immature neutrophils within total BM neutrophils (**F**) and
826 absolute counts of BM immature (left) and mature (right) neutrophils (**G**)**.** (**H**) CXCR2
827 expression on immature neutrophils shown as fold-change relative to BL controls. (**B-D** and **F-**
828 **H**) Data are shown as mean ± SEM. One-way ANOVA with Bonferroni *post hoc* test, ****p* < 0.01,
829 *****p* < 0.001, and ******p* < 0.0001. BL *n* = 10, oc-SO *n* = 12 and *n* = 9 (**B-D**), BL *n* = 11, oc-MI *n*
830 = 12, and oc-MI *n* = 10 (**F-H**). ns, non-significant; Neu, neutrophils; mNeu, mature neutrophils;
831 iNeu, immature neutrophils.
832

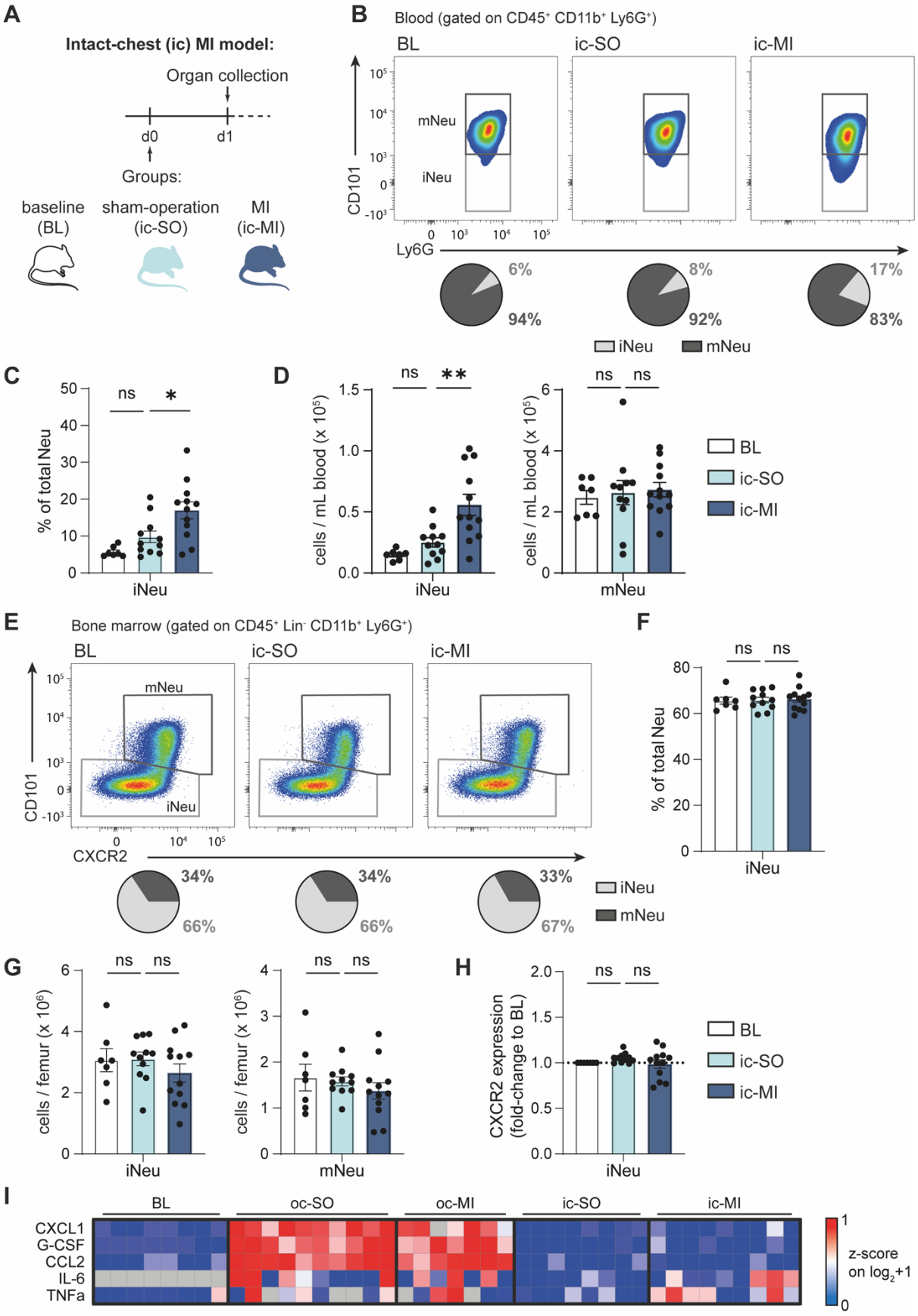

833 **Figure 3. Intact-chest MI induces a moderate increase of circulating immature neutrophils.**

834 (**A**) Experimental design of the intact-chest (cc) MI model. Mice were untreated as baseline
835 controls (BL, white), sham-operated (SO, light blue), or subjected to LAD coagulation (MI, dark
836 blue). Blood and bone marrow (BM) were collected 24h post-intervention for flow cytometric
837 analysis. (**B**) Representative flow cytometry analysis to identify neutrophil subsets in blood.
838 Pie charts indicate the average proportion of $CD101^+$ mature and $CD101^-$ immature subsets
839 within total circulating neutrophils. (**C-D**) Frequency of immature neutrophils within total
840 blood neutrophils (**C**) and absolute counts of circulating immature (left) and mature (right)
841 neutrophils (**D**). (**E**) Representative flow cytometry analysis to identify neutrophil subsets in
842 BM. Pie charts indicate the average proportion of $CD101^+$ mature and $CD101^-$ immature
843 subsets within total BM neutrophils. (**F-G**) Frequency of immature neutrophils within total BM
844 neutrophils (**F**) and absolute counts of BM immature (left) and mature (right) neutrophils (**G**).
845 (**H**) CXCR2 expression on immature neutrophils shown as fold-change relative to BL controls.
846 (**I**) Plasma levels of CXCL1, G-CSF, CCL2, IL-6, and TNFα. Analyte concentrations were
847 quantified by multiplex immunoassay, $\log_2(+1)$ transformed, and visualized as row z-scores.
848 Grey boxes indicate values below the detection limit. (**B-D** and **F-H**). Data are shown as mean
849 ± SEM. One-way ANOVA with Bonferroni *post hoc* test, $*p < 0.05$ and $**p < 0.01$. BL $n = 7$, ic-
850 SO $n = 11$, and ic-MI $n = 12$. ns, non-significant; BL, baseline; Neu, neutrophils; mNeu, mature
851 neutrophils; iNeu, immature neutrophils.
852

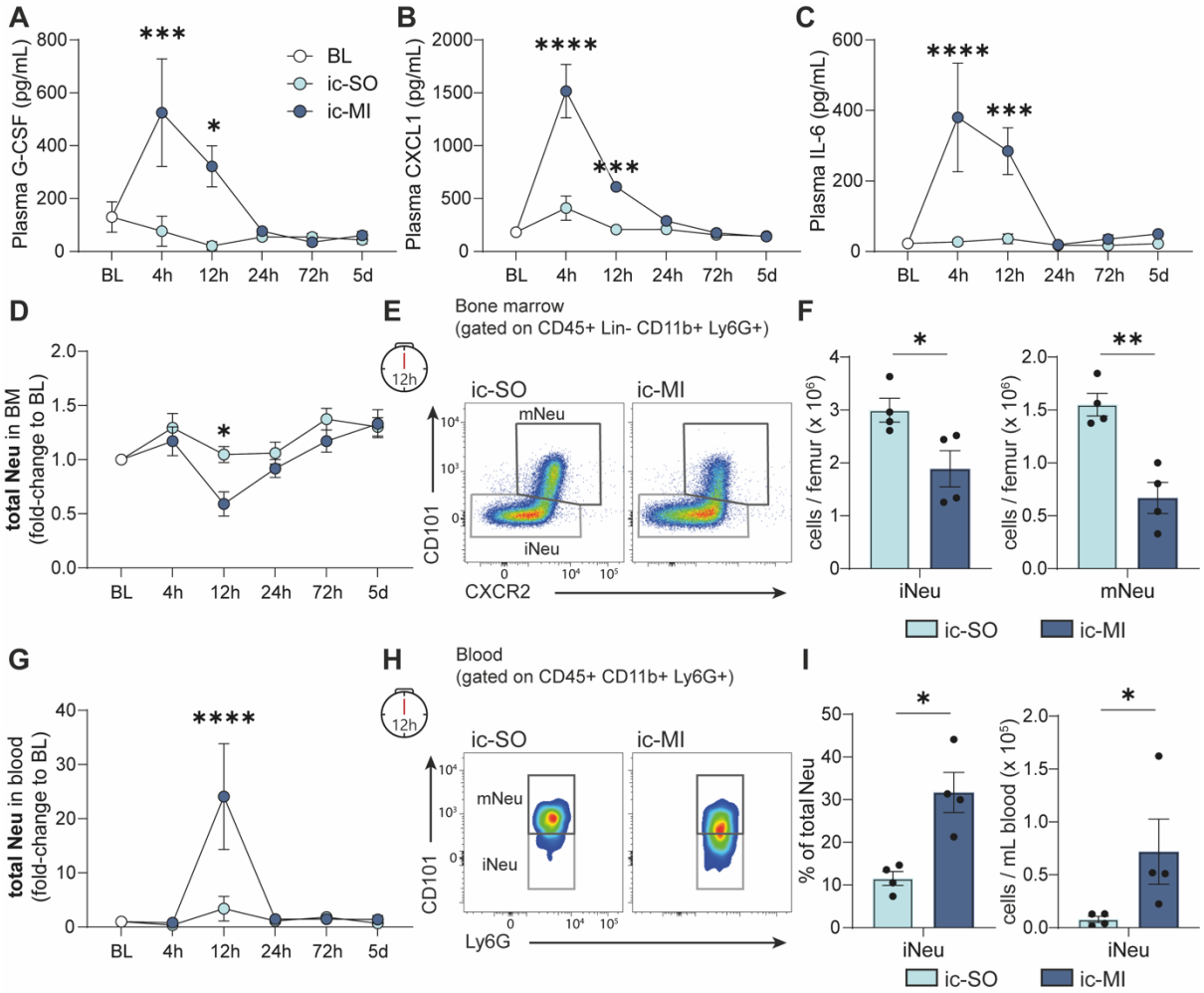

Figure 4. Dynamics of neutrophil response in the intact-chest MI model.

In the intact-chest (cc) model, mice were sham-operated (ic-SO, light blue) or subjected to myocardial infarction (ic-MI, dark blue). Samples were collected at the indicated time points. (**A-C**) Time course of plasma levels of G-CSF, CXCL1 and IL-6 in ic-SO and ic-MI mice. Analyte concentrations were measured by ELISA. (**D**) Time course of bone marrow (BM) neutrophils in ic-SO and ic-MI mice normalized to counts of corresponding BL controls. (**E**) Representative flow cytometry analysis to identify BM neutrophil subsets 12h post-intervention. $CD101^+$ neutrophils were considered mature, $CD101^-$ neutrophils immature. (**F**) Quantification of immature (left) and mature (right) BM neutrophils 12h post-intervention. (**G**) Time-course of circulating neutrophils in ic-SO and ic-MI mice normalized to counts of corresponding BL controls. (**H**) Representative flow cytometry analysis to identify blood neutrophil subsets 12h post-intervention. $CD101^+$ neutrophils were considered mature, $CD101^-$ neutrophils immature. (**I**) Fraction of total neutrophils (left) and counts (right) of immature neutrophils in blood 12h post-intervention. (**A-D** and **G**) Data are shown as mean ± SEM. Two-way ANOVA with Šidák *post hoc* test; *$p < 0.05$, *** $p < 0.001$, and ****$p < 0.0001$. (**A-C**) n = 3-6 per time

869 point per group, except ic-SO 24h *n* = 7 and ic-MI 24h *n* = 11. (**D** and **G**) *n* = 4-7 per time point
870 per group, except ic-SO 24h *n* = 11 and ic-MI 24h *n* = 12. (**F** and **I**) Data are shown as mean ±
871 SEM. Mann-Whitney or Welch's *t*-test. *$p < 0.05$ and **$p < 0.01$. ic-SO *n* = 4 and ic-MI *n* = 4.
872 ns, non-significant; BL, baseline; Neu, neutrophils; mNeu, mature neutrophils; iNeu,
873 immature neutrophils.
874

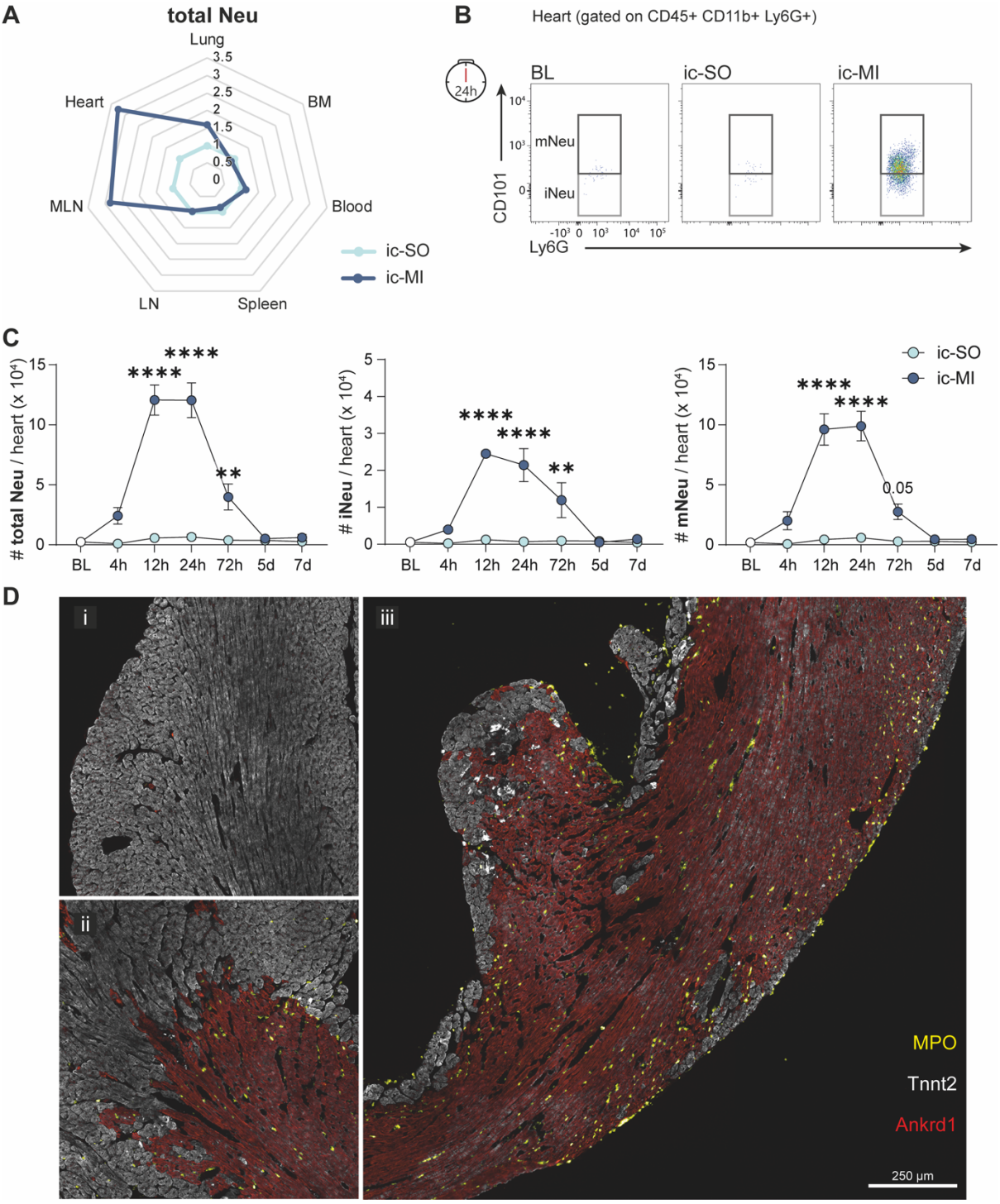

Figure 5. Infiltration of immature neutrophils in the infarcted heart in the intact-chest model.

(**A**) Radar plot showing neutrophils distribution in organs 24h post-intervention in ic-SO and ic-MI mice. Values for ic-MI (dark blue) are expressed as fold-change relative to ic-SO (light blue). Neutrophils were measured by flow cytometry. *n* = 4-12 per organ per group. (**B**) Representative flow cytometry plots of neutrophil subsets in heart 24h post-intervention in ic-SO and ic-MI mice. (**C**) Time course of cardiac neutrophil infiltration. Absolute counts of

883 total (left), immature (middle) and mature (right) neutrophils in the heart of ic-SO (light blue)
884 and ic-MI (dark blue) mice at the indicated time points post-intervention. Data are shown as
885 mean ± SEM. Two-way ANOVA between ic-SO and ic-MI groups for each time-point corrected
886 with Šidák *post hoc* test; $^{**}p < 0.01$ and $^{****}p < 0.0001$. n = 3-5 per time point per group
887 except ic-MI 24h n = 8. (**D**) Representative SeqIF images of mouse heart cross-sections 24h
888 post ic-MI, stained for neutrophils (MPO), healthy (Tnnt2) and stressed cardiomyocytes
889 (Ankrd1). Insets show (i) remote, (ii) border and (iii) infarct zone. Scale bar: 250 µm. ns, non-
890 significant; BL, baseline mice; ic-SO, intact-chest sham-operation; ic-MI, intact-chest
891 myocardial infarction; Neu, neutrophils; mNeu, mature neutrophils; iNeu, immature
892 neutrophils; BM, bone marrow, LN, peripheral lymph nodes; MLN, mediastinal lymph nodes.
893

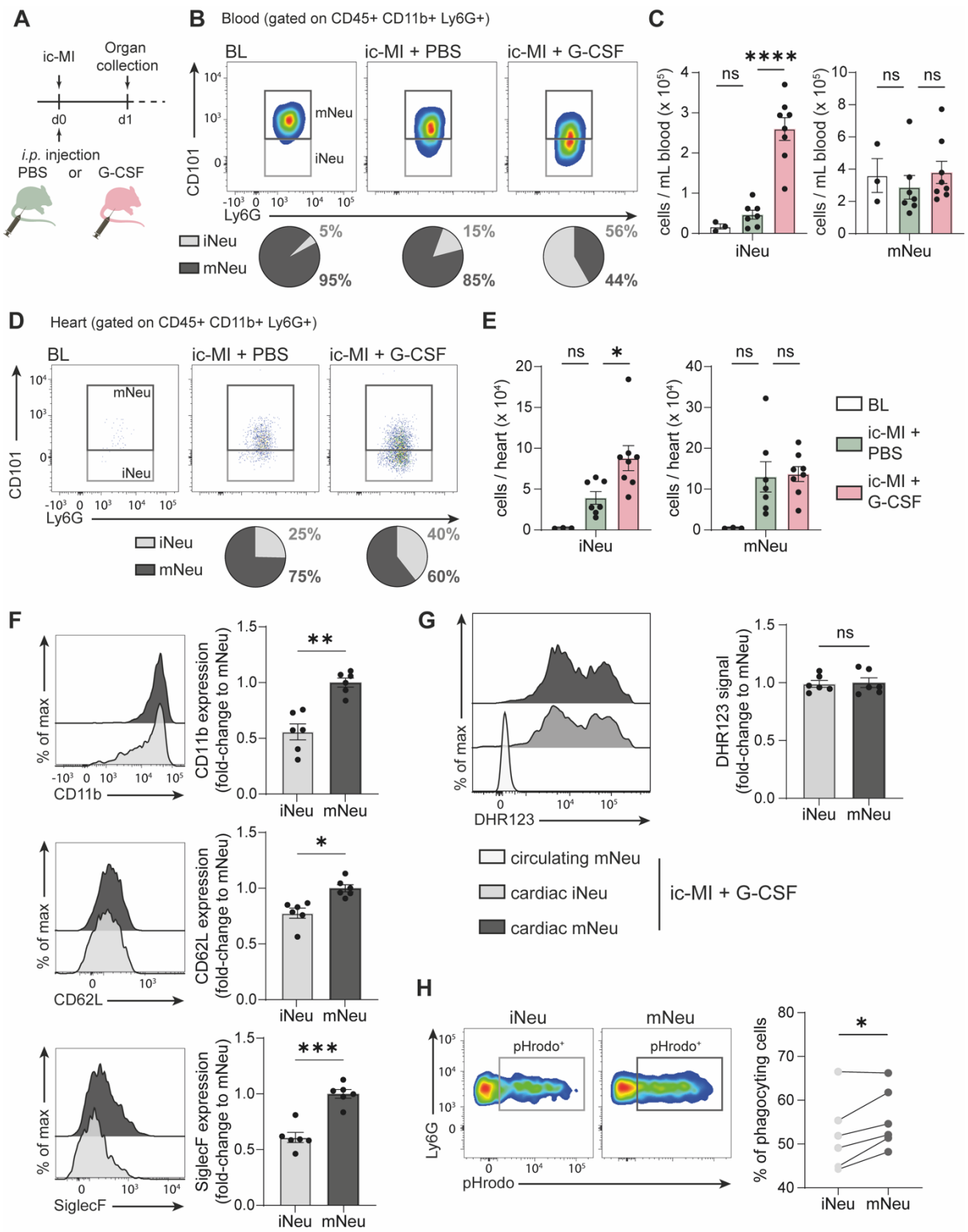

Figure 6. G-CSF promotes immature neutrophils infiltration into the infarcted heart. (**A**) Schematic of the experiment design. Mice were subjected to ic-MI and injected with either PBS (green) or G-CSF (red). Blood and hearts were collected 24h post-MI. (**B**) Representative flow cytometry analysis to identify circulating neutrophil subsets. Pie charts indicate the average proportion of CD101^{+} mature and CD101^{-} immature subsets within total circulating

900 neutrophils. (**C**) Absolute counts of circulating immature (left) and mature (right) neutrophils
901 from ic-MI mice treated with PBS (*n* = 7) or G-CSF (*n* = 8). (**D**) Representative flow cytometry
902 analysis of neutrophil subsets in the heart. Pie charts indicate the average proportion of
903 $CD101^+$ mature and $CD101^-$ immature subsets within total cardiac neutrophils. (**E**) Absolute
904 counts of immature (left) and mature (right) neutrophils in infarcted hearts from ic-MI mice
905 treated with PBS (*n* = 7) or G-CSF (*n* = 8). (**F**) Expression of CD11b, CD62L, and SiglecF on
906 cardiac immature (light grey) and mature (dark grey) neutrophils 24h after ic-MI in G-CSF-
907 treated mice. Representative flow cytometry histograms (left) and quantitative analysis
908 shown as fold-change relative to mNeu (right). (**G**) ROS production by cardiac immature (light
909 grey) and mature (dark grey) neutrophils 24h after ic-MI in G-CSF-treated mice.
910 Representative flow cytometry histograms of DHR123 fluorescence (left) and quantitative
911 analysis shown as fold-change relative to mNeu (right). Circulating neutrophils (white) were
912 used as controls. (**H**) Phagocytosis capacity of cardiac immature and mature neutrophils 24h
913 after ic-MI in G-CSF-treated mice. Representative flow cytometry histograms of pHrodo
914 particle uptake (left) and quantitative analysis, expressed as the percentage of pHrodo-
915 positive cells (right). (**C** and **E**) Data are shown as mean ± SEM. One-way ANOVA with
916 Bonferroni *post hoc* test; $*p < 0.05$ and $****p < 0.0001$. BL *n* = 3, ic-MI+PBS *n* = 7, ic-MI+G-CSF
917 *n* = 8. (**F**, **G** and **H**) Data are shown as mean ± SEM. Paired *t*-test with Holm-Šidák *post hoc* test;
918 $*p < 0.05$ and $**p < 0.01$. Cardiac immature and mature from ic-MI+G-CSF with each *n* = 6. ns,
919 non-significant. BL, baseline mice; ic-MI, intact-chest myocardial infarction; Neu, neutrophils;
920 mNeu, mature neutrophils; iNeu, immature neutrophils.
921

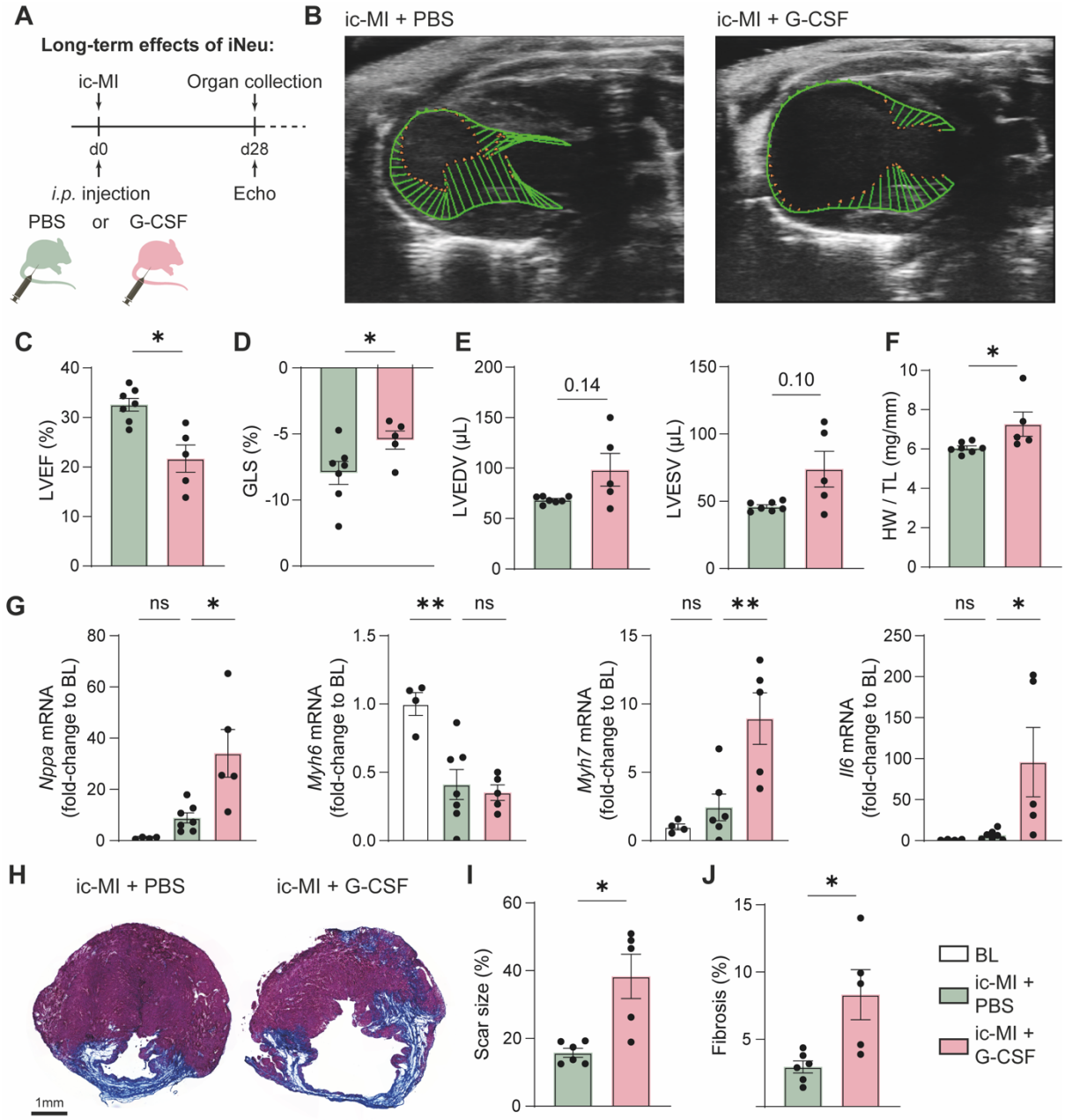

Figure 7. Cardiac immature neutrophil accumulation drives adverse myocardial remodeling. (**A**) Schematic of the experiment design. Mice were subjected to ic-MI and injected with either PBS (green) or G-CSF (red). Echocardiography and organ collection were performed 28 days post-MI. (**B-E**) Echocardiographic assessment of cardiac function in ic-MI mice treated with PBS (n = 7) or G-CSF (n = 5). (**B**) Representative images of strain analysis and quantification of (**C**) left ventricular ejection fraction (LVEF), (**D**) global longitudinal strain (GLS), (**E**) left ventricular end diastolic volume (LVEDV) and end systolic volume (LVESV). (**F**) Heart weight (HW) to tibia length (TL) ratio in ic-MI mice treated with PBS or G-CSF. (**G**) Cardiac mRNA expression of *Nppa*, *Myh6*, *Myh7* and *Il6* measured by qPCR and shown relative to baseline

932 (BL) expression. (**H-J**) Representative images of heart section stained with Masson's trichrome
933 (**H**) and quantification of infarct size (**I**) and fibrosis (**J**). Data are shown as mean ± SEM.
934 Welch's *t*-test (**C, D**, **E**, **I** and **J**) or Mann-Whitney (**F**) or One-way ANOVA with Bonferroni *post*
935 *hoc* test (**G**); * $p < 0.05$, ** $p < 0.01$ and *** $p < 0.001$. (**C-J**) BL $n = 4$, ic-MI+PBS $n = 6$-7, and ic-
936 MI+G-CSF $n = 5$. Scale bar: 1 mm. ns, non-significant. BL, baseline mice; ic-MI, intact-chest
937 myocardial infarction.
938

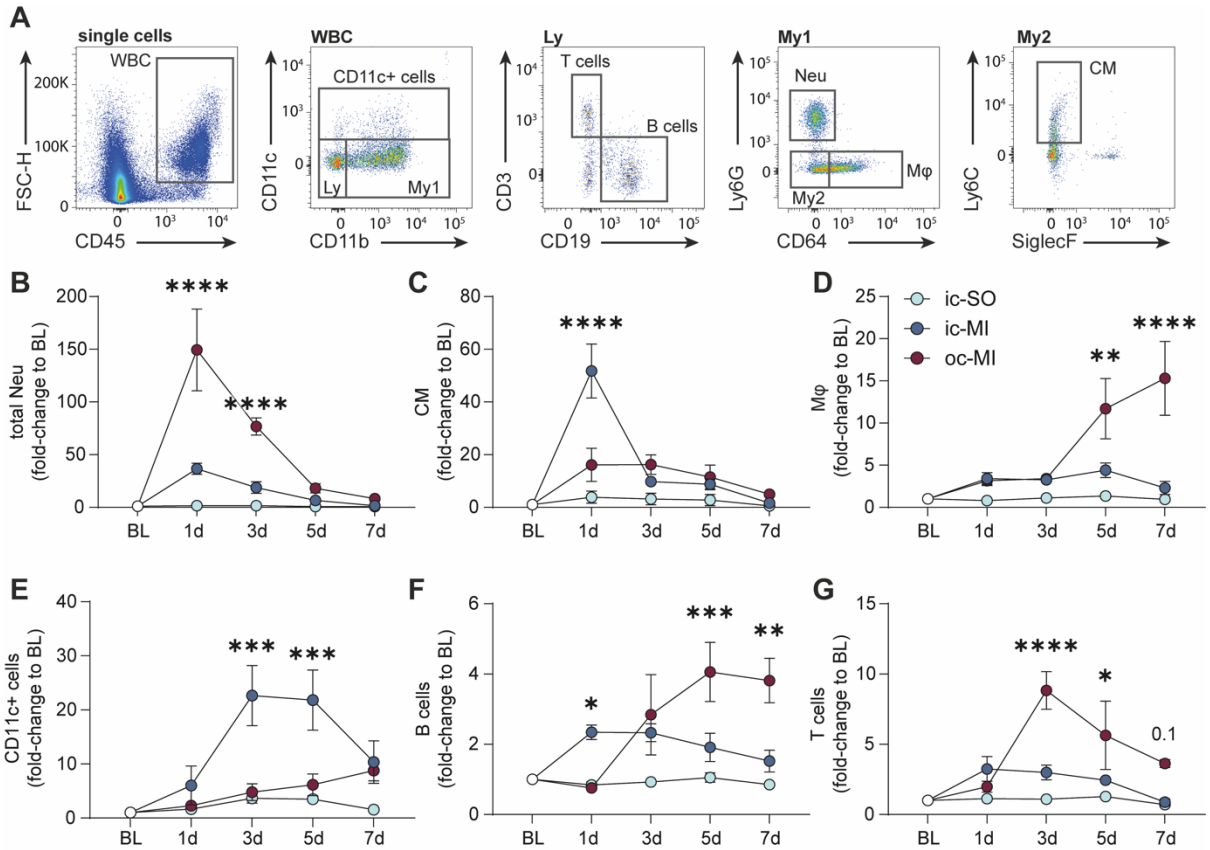

Figure 8. Immune landscape of the infarcted heart.

Mice were subjected to myocardial infarction using either the open-chest (oc-MI, dark red) or intact-chest model (ic-MI, dark blue). Some mice were sham-operated (ic-SO, light blue). Hearts were collected at the indicated time points (**A**) Representative flow cytometry analysis to identify cardiac leukocyte subsets in heart sample following ic-MI. (**B-G**) Time courses of cardiac neutrophils (**B**), classical monocytes (**C**), macrophages (**D**), CD11c^{+} cells (**E**), B cells (**F**), and T cells (**G**). Each leukocyte population in ic-SO (light blue), ic-MI (dark blue), and oc-MI mice (red) is expressed as fold change to baseline controls (BL). Data are shown as mean ± SEM. Two-way ANOVA with Tukey's *post hoc* test with *$p < 0.05$, **$p < 0.01$, ***$p < 0.001$ and ****$p < 0.0001$. n = 3-7 per time point per group except ic-MI 24h n = 10. CM, classical monocytes; MΦ, macrophages. ns, non-significant. BL, baseline mice; oc-MI, open-chest myocardial infarction; ic-SO, intact-chest sham-operation; ic-MI, intact-chest myocardial infarction.